University of Strathclyde

Control Strategy for constant-speed Wind Turbine in Below Rated Wind Speed

Investigation of a control strategy to improve power capture

Mohammad Aryanmanesh

Supervisor: Prof. William E. Leithead

MPhil Thesis

August 2019

"I hereby declare that this work has not been submitted for any other degree/course at this University or any other institution and that, except where reference is made to the work of other authors, the material presented is original and entirely the result of my own work at the University of Strathclyde under the supervision of Prof. William E. Leithead."

Acknowledgment

The author wishes to express his sincere gratitude to his supervisor Prof. Leithead, for his constant guidance and kind encouragement throughout the course of the research project. The generous supervision given by him was invaluable and reflected his comprehensive knowledge.

Also, the author would like to thank Dr. Hong Yu as his second supervisor, which he received tremendous support and help from her in many ways.

Contents

List of Figures

List of Tables

Abstract

The objective of this thesis is to design a control strategy to improve power capture in below rated wind speed for constant speed pitch regulated wind turbines.

To achieve the objective of this thesis, it is convenient to model rotor/wind-field interaction by a simple ordinary differential equation. It is also required to use a simple model to represent the dynamic behaviour of a grid connected constant speed horizontal axis wind turbine to assess the performance of the proposed control strategy.

Simulink based simulations of the wind model and turbine dynamics combined with the control strategy is performed to analyse its performance and to estimate the extra power capture by using the control system in below rated wind speed in comparison to running the turbine with fixed blade pitch angle (without the use of control strategy) in the same region.

Notations

α	Rectifier firing angle	(°)
β	Pitch angle	(°)
β_0	Optimum pitch angle	(°)
β_d	Pitch angle demand	(°)
λ	Tip-speed ratio	
λ_0	Optimum tip-speed ratio	
Ω	Rotor speed	(rad/s)
Ω_0	Rotational angular velocity	(rad/s)
$\Omega_r r$	Tangential blade element speed	(rad/s)
Ω_z	Zero-torque speed	(rad/s)
ρ	Density of air	(1.2256 kg/m^3)
γ	Turbulent wind speed decay factor	
γ_1	Low-speed shaft external damping coefficient	
γ_1^*	Low-speed shaft internal damping coefficient	
γ_2	High-speed shaft external damping coefficient	
γ_2^*	High-speed shaft internal damping coefficient	
θ_G	Rotational displacement of the gearbox	
θ_H	Hub angular/rotational displacement	
θ_R	In-plane rotor rotational displacement	
ϕ_H	Fore-and-aft angular displacement of the hub	
ϕ_R	Out-of-plane rotor rotational displacement	
σ_v	Wind turbulence intensity	
ω	White Gaussian noise	
ω_g	Generator speed	
A	Area	(m^2)
$A_{-\infty}$	Downstream cross-sectional area	(m^2)

A_∞ Upstream cross-sectional area (m^2)

A_D Disc area (m^2)

C_P Power coefficient

C_{pmax} Maximum power coefficient

C_Q Torque coefficient

C_T Thrust coefficient

D_{GB} Gearbox mounting

D_T Fore-and-aft damping force (N)

F Force (N)

F_1 In-plane rotor aerodynamic torque (N.m)

F_2 Out-of-plane rotor aerodynamic torque (N.m)

f_D Drag force (N)

f_L Lift force (N)

h Height of the rotor (m)

I_1 Rotor inertia (kg. m^2)

I_2 Generator inertia (kg.m^2)

J_c Tower/Rotor cross-coupling inertia (kg.m^2)

J_H^* Hub inertia (kg. m^2)

J Rotor inertia (kg.m^2)

J_T Total moment of wind turbine inertia (kg.m^2)

J_X Tower/Gearbox cross-coupling inertia (kg.m^2)

K_1 Low-speed shaft stiffness (kg/s^2)

K_2 High-speed shaft stiffness (kg/s^2)

K_E Edge-wise stiffness (kg/s^2)

K_F Flap-wise stiffness (kg/s^2)

K_T Tower stiffness (kg/s^2)

L Length scale of the turbulence

m	Mass	(kg)
N	Gearbox ratio	
P	Power	(kW)
P_{av}	Available power	(kW)
P_g	Generated power	(kW)
R	Radius of rotor	(m)
R_c	Distance from the hub to the centre of blade mass	(m)
T	Torque	(kN.m)
T_D	Drive-train torque	(kN.m)
T_{dem}	Demanded torque	(kN.m)
T_e	Generator torque	(kN.m)
T_f	Aerodynamic torque	(kN.m)
$\hat{T}_f$	Estimated aerodynamic torque	(kN.m)
V	Wind speed	(m/s)
$\hat{V}$	Mean wind speed	(m/s)
$V_{-\infty}$	Downstream wind speed	(m/s)
V_{rel}	Relative speed	(m/s)
T_A	Axial hub torque	(N.m)

1. Overview

1.1. Introduction

The interest to generate electricity from renewable resources has increased significantly due to concern about the environment. Wind power can be considered as one of the most promising energy sources to directly generate electrical power by using wind turbines.

Generating electricity from wind turbines goes back to the late nineteenth and early twentieth century, initially for battery charging for remote dwellings [19].

After the development of vertical axis wind turbines with narrow curved blades designed by Darrieus in 1920, wind turbines progressed rapidly with new axis, rotor and blade design concepts.

In the 1970's constant speed wind turbines with 100kW rated power were developed in Germany, which had a rotor diameter of 15m. Since then the technology of wind turbines has improved dramatically to the point where 5MW wind turbines are proposed for offshore wind farms [19].

1.2. Thesis structure

The thesis is organised as follow:

Chapter 1, a brief introduction is presented in this chapter as well as description of the thesis structure.

Chapter 2, this chapter provides some general information about renewable energy, renewable energy use and electricity production from renewables in the UK and some brief information about wind energy and wind turbines.

Chapter 3, in this chapter the work that has been completed or proposed previously by other researchers in the same area of interest of this thesis is discussed.

Chapter 4, this chapter provides the mathematical representation of a wind model as well as a simple wind turbine dynamics model.

Chapter 5, this chapter describes the implementation of the wind and the turbines dynamics model represented in chapter 4, in Matlab/Simulink.

Chapter 6, in this chapter a detailed description of the proposed control strategy is provided, and it also describes the implementation of the control strategy in Matlab/Simulink in combination with the rest of the model previously implemented.

Chapter 7, this chapter presents the results of the simulations carried out to assess the performance of the control strategy compared to the simulation of the same model under the same conditions with no control system employed, estimation of the power capture and annual energy yield and also draws some conclusions of the research.

Chapter 8, finally this chapter presents the conclusion of the research.

2. Background

2.1. Renewable energy

Renewable energy sources, which can be interpreted as vast sources of energy arising from the sun's radiation, have always been used by humanity from ancient times to the most modern time.

Renewable energy can be classified into different categories, such as:

- **Solar radiation:** the energy from heat and light present in the sun's radiation can be obtained either directly as heat or, by using different conversion techniques such as photovoltaic (PV), converted to electrical power.
- **Water and Hydropower:** in this type of renewable energy resource, turbines and generators make use of the energy of flowing water to generate electricity. This technique can be referred to as the first large scale electricity generation source.
- **Wave and Tidal:** this type of resource has been developed more recently. Water flow rotates the blades inside water turbines which rotate the shaft that is connect to a generator to produce electricity as presented in Figure 2-1:

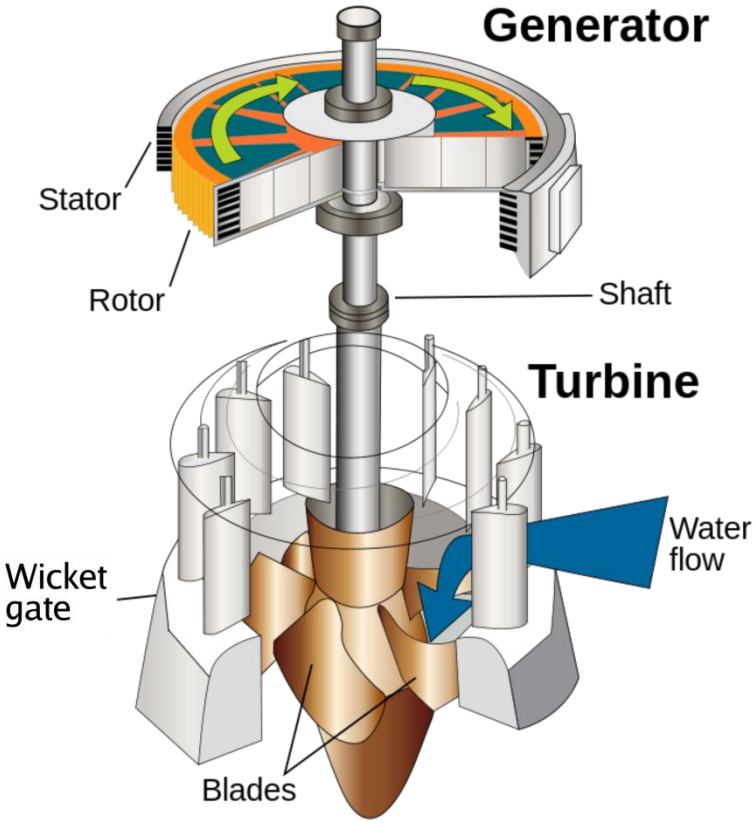

Figure 2-1 : Water Turbine

- **Wind:** wind has always been considered as one of the main energy sources. In early centuries wind energy was used by windmills and wind pumps as rotational energy to mill grain or pump water, and more recently for electricity generation.
- **Geothermal:** this type of energy source can be referred to as the only independent form of renewable energy from the sun. The heat that has naturally been produced within the earth can be exploited directly for heat production or converted to electricity using steam turbines.
- **Bioenergy:** in this type of resource energy would be derived from biological materials, which were living relatively recently compared to fossil fuels. Heat and power can be produced by burning the biomass. Although carbon dioxide will be released to the atmosphere throughout this process, the same amount of carbon dioxide would be absorbed from the atmosphere while these biological materials were growing. Therefore, the whole cycle of biological renewable can be considered to be carbon neutral [6].

Historical development of renewable energy goes back to at least 3000 years, generally to the use of wind mills for different purposes such as grinding grains and pumping water. However, from the 18th century, the use of windmills declined as fossil fuelled engines became available. This was followed by the increase of electrification throughout cities.

The sustainability of fossil fuels has been a factor that encouraged the development of renewable energy in the last few decades. Ideally, an energy source can be referred to as "sustainable" if does not come to an end by constant use, does not involve environmental problems such as pollutant emissions, and does not lead to major health hazards.

The contribution of renewable energy to world total energy consumption in 2008 was 19%. This quantity comprises all type of renewable energy resources such as hydropower, biomass, solar, wind energy and geothermal, with different proportions as demonstrated in Figure 2-2:

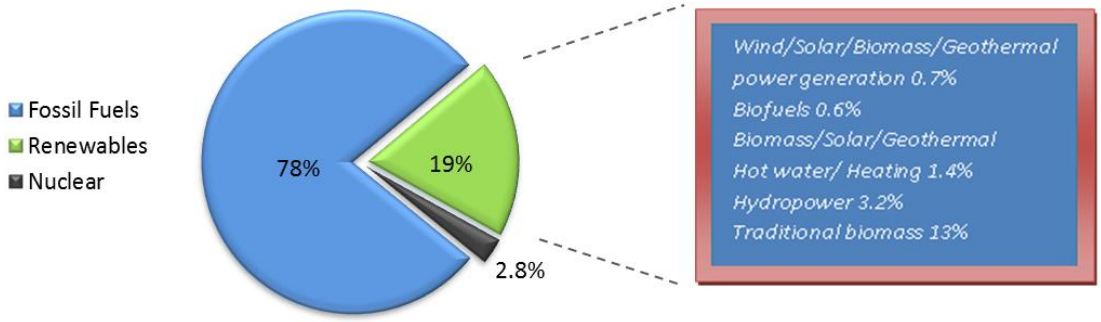

Figure 2-2: Contribution of renewable energy in the world energy consumption

The capacity of global renewable power was estimated in 2009, to be 1230 GW with a 7% increase from 2008. Worldwide wind power capacity has the biggest increase, by 38 GW, amongst all renewable resources. With this 41% growth over 2008, wind power capacity installed worldwide reached a total of 159 GW [20].

The main issue considered to be the motivating factor for renewable energy growth is global warming. Concern over this vital environmental problem resulted in promotion of carbon-free technologies using a range of policy efforts.

World governments have discussed solutions to reduce the rise of carbon dioxide emissions. A general target was set in December 1997 from international climate change negotiations, supported by the United Nations. The target agreed is a reduction of greenhouse gases by 5% between 1990 and the completion date of 2008-12. The European Union members have also agreed on a target of 8% emissions reduction, and a reduction of 12.5% was the target set for the United Kingdom over the same period [6].

Related to renewable energy, 55 countries have set different types of promotion policy as well as policy targets in 2005. This figure was significantly increased to over 100 countries by early 2010.

2.1.1. Renewable energy development in the UK

The presence of natural fossil fuel resources was the main reason for the UK being less motivated to develop renewable resources. Therefore, the UK is facing a great challenge to meet the 2020 targets, which states that 15% of the energy consumption in the UK should be generated from renewable resources. Consumption of renewable energy in the UK was only 2.25% in 2008 [6] and an increase of approximately a factor of seven must take place in just over a decade.

The main purpose of this fast conversion to renewable energy by 2020 would be, apart from security of the UK's energy system and less dependence to imported fossil fuels, to meet the target of CO2 emission reduction by 50%.

The main strategy proposed achieve the stated goals involves meeting a portion of the different energy consumption from renewable energy. This strategy aims to achieve the following objectives:

- 30% production of the UK's electricity from the renewable resources, which indicates a significant increase from current production of around 5.5%.
- 12% production of heat from the renewable resources such as biogas, solar and biomass.
- 10% production of transport power from the renewable resources, which would involve the electrification of the rail network to increase the current contribution of around 2.6% [21].

2.1.2. Electricity generation from renewables in the UK

Electricity generation can be considered as the main product of the renewable energy being 71% of the renewable energy production in 2009. This figure is similar to 2008. However, faster growth of Biofuels production for transport caused a decrease from 83% and 79% in 2006 and 2007, respectively.

The total electricity production in 2009 was 3421 GWh, which indicates a 17% growth compared to 2008. This amount of increase can be broken down into key technologies. The main contributors are summarised below:

- Onshore wind turbines generated 1772 GWh, increased by 31% from 2008.
- Offshore wind turbines generated 435 GWh, increased by 33% from 2008.
- 541 GWh was generated from plant biomass, increased by 95% from 2008.
- 285 GWh was generated by combustion of biodegradable municipals solid wastes, an increase of 23% from 2008.
- Landfill gas generated 195 GWh, increased by 4% from 2008.
- 193 GWh was generated by co-firing of biomass with fossil fuels, increased by 12% from 2008 [21].

Wind energy, onshore and offshore, produced the most energy output among the renewable technologies in 2009. Wind turbines generated 37% of the overall electricity produced by renewable resources, hydro source produced 21%, landfill gas produced 20%, co-firing technology produced 7% and other biomass generated 15% of the total electricity generation.

However, in 2010 the provisional figures did not demonstrate an impressive growth, as the total electricity generation from renewables was 3558 GWh. This amount was increased only by 4% compared to 2009. Due to its development in capacity of offshore wind turbines, there was a 75% increase in electricity generation from this source [6]. But an 8% decrease was observed in onshore wind generation, due to presence of lower wind speeds in 10 months of 2010 compared to 10 years average, and 32% in hydro power because of lower rainfall.

The total installed renewables capacity was 9021 MW at the end of 2009, an increase of 12%, from 8031 MW in 2009. This increase comprises of a 476 MW increase in onshore wind turbine capacity and 400 MW increase in offshore wind turbine capacity [20].

2.2. Wind resource

Variations in atmospheric pressure, which occur as a result of unbalanced solar heating of the earth's surface, cause air mass movement and is referred to as wind. Air behaves in the exact same manner as all other gases, expanding when heated and contracting when cooled. This behaviour results in warmer air having less density than cooler air, therefore being lighter and rising to high altitudes. Cooler air then flows in to replace the rising air.

Wind energy can be considered as the fastest growing technology of all the electricity generation sources in the world. Wind is completely sustainable and with established advanced technology it aims to develop into a significant energy source for the future.

With different levels of success, since the end of 19th century, continuous challenges to producing electricity from wind energy have been addressed, initially by small wind turbines charging batteries.

Extracting energy from wind and gaining a robust understanding of wind energy conversion systems requires knowledge in various fields such as, meteorology, electricity and structural and mechanical engineering.

2.2.1. Characteristics of the wind

Wind energy exploitation depends on a reliable understanding of the nature of the wind. This is critical to all areas of this field such as appropriate siting of wind farms, design of wind turbines and their effect on the electricity distribution networks.

Of all characteristics of the wind resource, its variability, both temporal and geographical, can be considered the most noticeable one.

If variability of wind is explored on a large scale, various climatic regions will be observed in the world, due to the latitude. On a smaller scale, the study of each climatic region demonstrates a large amount of variation, due to physical geography. Physical geography comprises factors such as the ratio of dry land to sea, existence of high lands such as mountains and size of land masses. Also, another geographical factor that can have a considerable influence on the regional variation is the type of plants due to their absorption or reflection of solar radiation and the changes they cause to surface temperatures and on humidity.

The study of local wind illustrates that wind climate is significantly affected by the landscape as wind velocity is greatly reduced by obstacles and the wind experienced on high grounds such as top of mountains is a lot more compared to sheltered valleys.

Temporal variability at a specific location can be investigated on different scales. On a large scale the amount of variation from year to year is being studied and on even larger scale the study can be over periods of decades. However, these large scales do not produce accurate predictions.

Shorter time-scale variations such as seasonal variations are better understood and can produce more reliable predictions for development of wind farms for instance. These variations can be predicted a few days ahead and are known as synoptic variations.

Different locations may also illustrate variations with time of day, which are referred to as diurnal variations and can be predicted. Wind speed variations on even shorter time-scale of minutes, seconds or less are known as turbulence and should be carefully considered when designing the turbines as they can have a major impact on their performance as well as the power quality transferred to the grid.

2.3. Wind turbine

A modern wind turbine consists of several different components that each performs a particular task in the operation of a wind turbine. These components are:

Nacelle, rotor blades, hub, low speed shaft, gear box, high speed shaft with its mechanical brake, electrical generator, yaw mechanism, electronic controller, hydraulic system, cooling unit, tower, anemometer and wind vane, as shown in Figure 2-3.

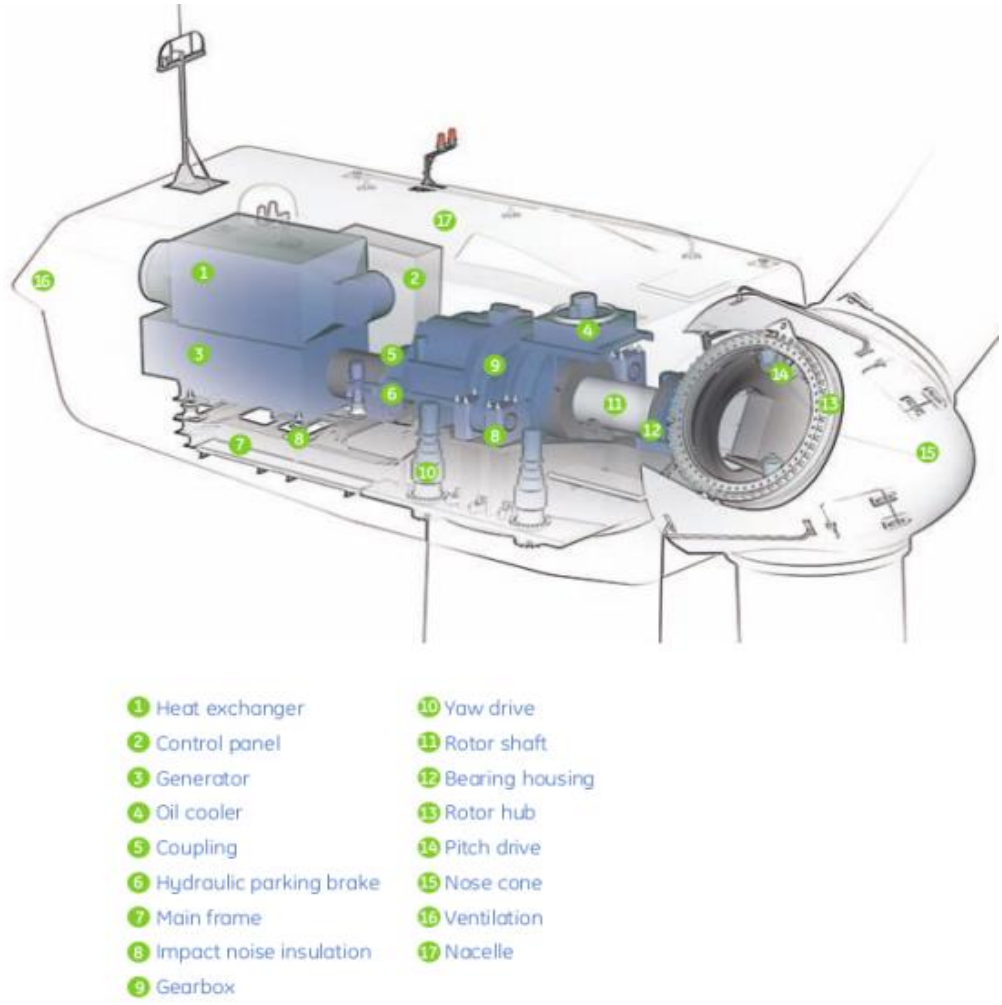

Figure 2-3: Wind turbine components

The rotor is connected to the main shaft and if there is enough wind to rotate the rotor the shaft will start rotating. The shaft is connected to a gearbox which would convert the approximately 22 rmp rotation of the low speed shaft to 1500 rmp, since the generator has to turn at this speed to generate electricity. The gearbox turns the generator using the high-speed shaft. The generator needs to be cooled down when it is running because during its operation it produces so much heat which could damage the components. The task of the yaw mechanism is that to turn the nacelle in a way that the rotor faces the wind. A controller acquires information about the wind direction from the wind vane and then operates the yaw mechanism to turn in the appropriate direction. The controller also controls some other parts of wind turbine such as allowing the rotor to start running when the anemometer informs it that there is sufficient wind to start functioning, i.e. the cut in wind speed is reached. The mechanical brakes will be used on occasions that the wind turbine needs to be serviced or repaired so it would be guaranteed that the rotor would not start rotating.

2.4. Wind turbine types

Fundamentally, there are two types of wind turbine which are constant speed and variable speed wind turbines.

2.4.1. Constant speed vs variable speed wind turbines

Initially, most wind turbines were designed to operate at constant speed during power production. The generator of constant speed wind turbines is connected directly to the grid. Hence, the rotation speed of the rotor is fixed to the frequency of the grid.

During the start-up procedure, the rotor is accelerated by the wind to reach the required speed. Once the required speed is reached, the turbine is connected to the electricity grid with the rotor speed being kept constant. For this reason, this type of wind turbine is referred to as a constant speed wind turbine.

Alternatively, variable speed wind turbines were designed. Variable speed operation is realised by connecting the generator to the grid indirectly through a rectifier and inverter. This allows separation of the rotor speed from the grid frequency which results in flexibility over matching the rotor and wind speed. Consequently, the rotor can retain better flow geometry providing better efficiency.

Even at low wind speeds (normally 4m/s) the rotor can be connected to the grid and then speed up in proportion to the increase in wind speed. As the speed of the rotor can vary, this type of wind turbine is referred to as a variable speed wind turbine.

It should be noted that in above rated wind speeds the variable speed rotor reverts to nearly constant speed operation for power regulation.

Even though there is a considerable cost for the power electronics required in variable speed wind turbines, in comparison between the two types, variable speed wind turbines offer significant advantages which outweigh the extra cost and makes this design more preferable over constant speed machines.

The two most significant advantages of variable speed wind turbines are:

- Maximising the energy capture in below rated wind speed
- Substantial load reduction in above rated

2.4.2. Power regulation

The two wind turbine types mentioned can also be divided into two different categories in terms of power regulation in above rated region (high wind speeds), which are **Stall** and **Pitch** regulation.

Pitch vs Stall regulation

The energy in the wind increases at almost the cube of the wind speed. High wind speeds are not frequent enough to economically justify designing the wind turbine to be most efficient at high wind speeds to extract the total energy available in that region. Therefore, it is preferred to

aerodynamically discard the extra energy in the wind and limit the power at a pre-defined wind speed, which is referred to as rated wind speed. The power produced at rated wind speed is referred to as rated power and is kept constant for any wind speeds above rated, until the wind speed reaches 25m/s (cut-out) which is too high for the wind turbine to operate. The wind turbine shuts down when the wind speed reaches the cut-out value.

Two methods are commonly employed to limit the excess power in above rated wind speeds. The first method is stall regulation, which works passively. The rotor blades are designed in a manner to stall when the wind speed reaches its rated value, therefore, limiting the generated power from increasing with the increase in wind speed.

With the rotational speed of the rotor being effectively constant in above rated region, an increase in wind speed causes the angle of attack to increase which results in stall, the lift to drop and drag to increase. This leads to a more inefficient lift to drag relationship and reduced driving torque.

In variable speed wind turbines, the rotor speed can be varied to intentionally bring the turbine to stall.

The second method for power limiting is pitch regulation which is an active process. On these types of wind turbine, the rotor blades have bearings. This allows the blades to rotate around their longitudinal axis during operation.

In above rated region, the blades are continuously pitched to the angle at which rated power is produced.

For pitch regulated wind turbines, the rotor speed and/or generator power must be continuously and precisely measured as they are the driving factors for adjusting the pitch angle.

Pitching the rotor blades provides more potential benefits other than power regulation. The blades can be adjusted with appropriate pitch angles to reduce the aerodynamic loads which reduce the thrust forces. This results in reduction of material and weight which makes the wind turbine more cost effective. Pitching the blades appropriately also reduces the fatigue loads which can extend the life time of the wind turbines.

3. Control overview

3.1. Wind turbine control system

Modern wind turbines need to be reliable and efficient and control systems play a vital part in achieving this goal. A suitably designed controller results in better extraction of wind energy as well as reduction of the fatigue loads that reduce the wind turbine lifetime.

The control system is a set of algorithms/software programs running on hardware ensuring that the turbine operates in the way that is intended and designed. The control system runs on a small computer, referred to as a PLC (short for Programmable Logic Controller) which is installed in the turbine's nacelle or tower base.

The control system can be split into two main parts according to the functionality: the supervisory controller and the dynamic controller as shown in Figure 3-1.

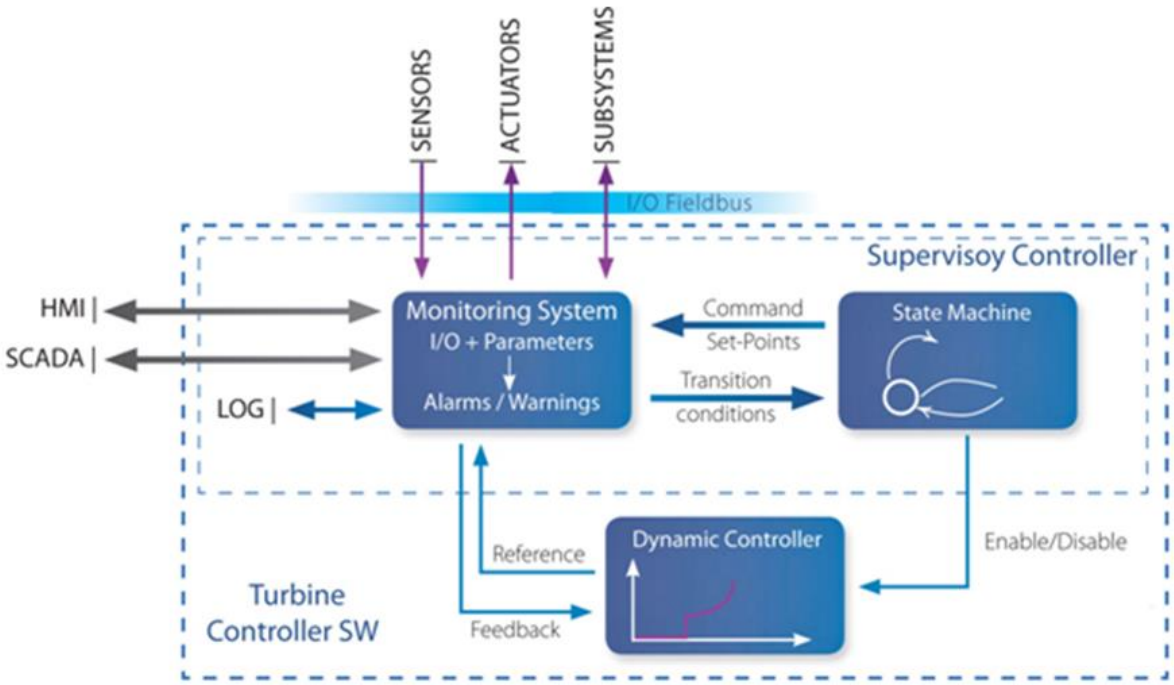

Figure 3-1: Wind turbine controller software

3.1.1. Supervisory controller

The supervisory controller manages the entire turbine's behaviour, ensuring the turbine operates in safe and stable conditions. It transits between different operational states, such as start-up, power production, shutdown etc. according to the monitored conditions and defined requirements. This involves receiving signals from the sensors installed on the turbine, going through a decision-making process and commanding the appropriate action.

Apart from the wind turbine's actions mentioned above, more actions are affected by the supervisory control. This includes enabling turbine dynamic controller for power regulation, engagement and disengagement of shaft and rotor brakes for parking and maintenance purposes as

well as commanding the subsystems such as cooling systems for different components or the yaw system etc.

The supervisory controller must ensure that pre-defined requirements are met and specific tasks are completed before transition to the next state or task. If these criteria are not met due to a fault or conflict, the supervisory is then responsible to issue the necessary alarms to notify the operator and take appropriate actions to shut down and bring the turbine to safe condition if required.

As shown in Figure 3-1, the supervisory controller also provides capability for human interaction with the turbine (manual operation or visualisation of the operating state and displaying data) via the SCADA (Supervisory Control and Data Acquisition) system or the HMI (Human Machine Interface).

3.1.2. Dynamic controller

The dynamic controller ensures steady power production and reduces lifetime damage of the turbine by continuously controlling the angle of the blades around its axis (referred to as pitch angle) and controlling the power.

The generic/high level objectives of the dynamic controller can be summarised to:

- Increase power capture
- Regulating power and reducing mechanical loads

Wind turbines are designed with a defined maximum power output (referred to as rated power), which varies between different designs, and one of the objectives of the dynamic controller is to ensure that the turbine will not exceed this limit to avoid fatal damage to the turbine. For example, if the wind speed is higher than the speed at which the turbine produces the maximum power, the control system pitches the blades to discard the excess energy in the wind.

However, when the wind speed is low (below the rated speed) the objective of the dynamic controller is to optimise the energy capture from the wind to produce a better power curve.

These objectives are highly dependent on the operating region of the wind turbine. By using a typical power curve shown in Figure 3-2, the different operating regions with reference to rated wind speed are illustrated.

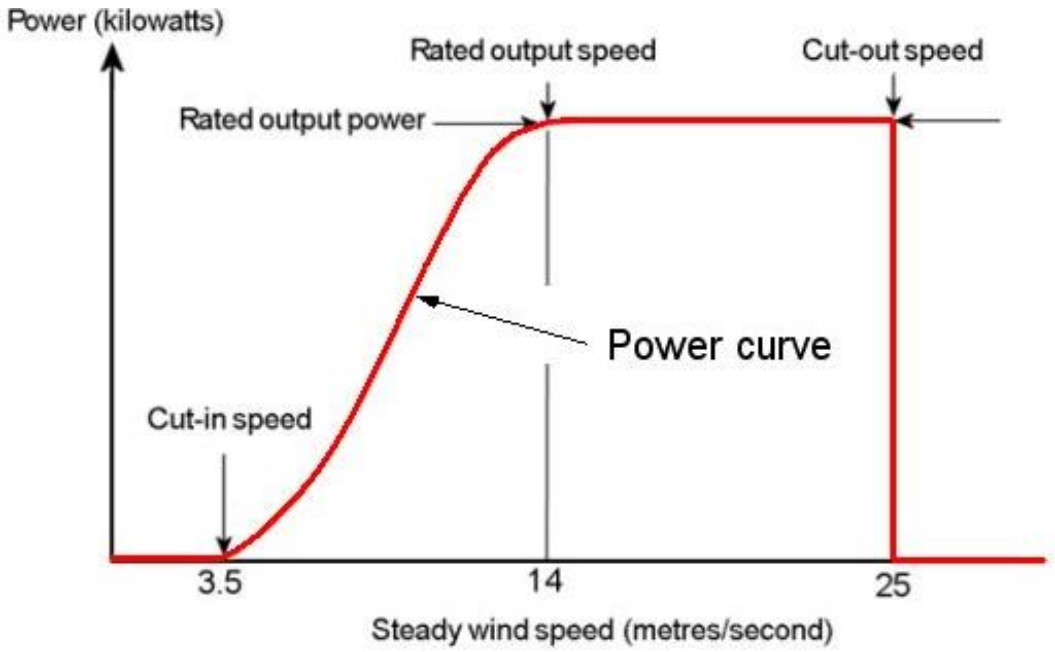

Figure 3-2: Typical wind turbine power curve with steady wind speed

3.2. Operational regions

As mentioned earlier the tasks of the controller differs depending on whether the wind turbine is operating below or above rated.

3.2.1. Below rated

The objective of the controller in the below rated region (low wind speed) is to extract as much power from the wind as possible.

To maximise the energy capture in this region, the variable speed wind turbines operate with minimum pitch angle. With the pitch angle fixed, the operating strategy chosen to maximise the energy capture is to track the maximum aerodynamic efficiency curve, known as the C_{p-max} curve. A suitably designed controller would track the C_{p-max} curve more accurately which results in more energy capture.

Variation in the rotor speed varies the aerodynamic efficiency for any given wind speed. Hence, the maximum efficiency is obtained at a unique point on the torque/rotor speed plane. These points are shown in Figure 3-3.

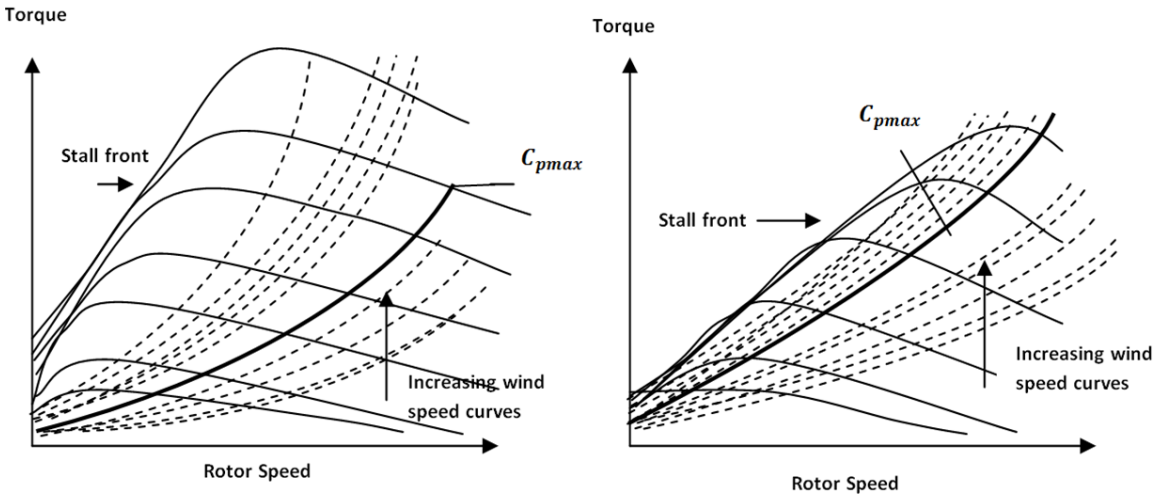

(a) Flat $C_p - \lambda$ curve

(b) Peaked $C_p - \lambda$ curve

Figure 3-3: Torque vs rotor speed curve with various efficiencies

(NOTE: see appendix A for more details about flat and peaked $C_p - \lambda$ curve)

The positions of the maximum aerodynamic efficiency points in Figure 3-3, is referred to as C_{p-max} as these points correspond to the maximum value of the aerodynamic power coefficient,C_p, [10].

By controlling the aerodynamic torque to track the C_{p-max} curve as accurately as possible, the energy capture can be maximised.

Three different control strategies can be employed to track the C_{p-max} curve in below rated wind speed [9], which are:

- Tracking by drive-train torque
- Tracking by aerodynamic torque
- Tracking by combined drive-train and aerodynamic torque

These control strategies are not discussed in depth in this thesis as the focus of this thesis is constant speed wind turbines.

The main focus of this thesis is constant speed wind turbines. Unlike the variable speed machines that keep the blade pitch angles at the minimum (referred to as fine pitch angle), in order to maximise the energy capture in this region, the blade pitch angles must vary to achieve the optimum angle of attack. This control strategy is discussed in detail in Chapter 6.

3.2.2. Above rated

In above rated region, apart from maintaining the power generation at its rated value, the controller includes other objectives, which are [5], [9], [18]:

- Compensation of aerodynamic nonlinearities
- Ensuring stability
- Tower and rotor load reduction

- Preventing from over speeding by maintaining generator speed and torque within the limit
- Preventing excessive pitch activity

All controller objectives must be considered when designing the controller as unavoidably there are trade-offs whereby improving the performance of one of the aspects can lead to undesirable effect on another objective. Therefore, overall performance of the controller must be considered.

There are several studies carried out with the purpose of improving control system performance by employing different techniques such individual pitch control.

As the focus of this thesis is below rated region the control strategies or methods in above rated are not explored any further.

4. Mathematical representation of dynamics

4.1. Wind model

The interaction of the rotor with the wind causes transient torques and moments, which determine the dynamics of Horizontal Axis Wind Turbines (HAWT). Therefore, the appropriateness of the wind model strongly impacts on the validity any dynamic analysis or assessment of performance of a wind turbine.

Wind turbine blades pass through a wind field, which is time varying in three dimensions. The structure of the wind field can be considered to consist of deterministic and stochastic components. The deterministic components are caused by tower shadow and wind shear, and the stochastic components are caused by wind speed turbulence.

When concerned with torque or moment, the wind speed variation over the swept disc can be reduced significantly by averaging over the blades. However, significant periodic components with frequencies equal to integer multiples of the rotational angular velocity,Ω_o, would be caused by the rotation of the rotor. Compared to the spectrum of the point wind speed, the outcome is that the power in the spectrum of the wind speed is significantly increased at integer multiples of Ω_o but reduced at other frequencies.

It can be observed that the spectral peaks also consist of stochastic and deterministic components similar to the wind field structure, and the stochastic component is typically the most significant.

When it is required to model only one torque or moment, the wind field can be represented by a scaled effective wind speed. This effective wind speed is the uniform wind speed over the rotor that causes the same aerodynamic forces as the non-uniform wind field. Using simple ordinary differential equations, the time variation of the effective wind speed can be modelled. It is possible to interpret the effective wind speed model as a filtered point wind speed.

The effective wind speed model [1] is derived by employing the method introduced by Madsen and Frandsen [2]. This method describes a single wind speed, which is an average of the wind field over the whole rotor disc that can be used to derive the total axis hub torque.

The effective wind speed model is not intended to represent spectral peaks, nor to represent deterministic components such as wind shear and tower shadow. It is only intended to represent the low frequency turbulent component. The very low frequency components of the turbulent fluctuations can be considered uniform over the rotor disc. Therefore, they form a slowly varying

quasi-static mean wind speed and the effective wind speed model can be derived by considering the perturbation in the wind-field relative to this quasi-static mean wind speed.

The axial hub torque,$T_A(t)$, that the wind induces on the blade is

$$T_A(t) = \int_A W\big(r, V(\boldsymbol{r}, t)\big) dA \tag{1}$$

Where $V(\boldsymbol{r}, t)$ is the wind speed field at the point $\boldsymbol{r}$ and at time t,

W is a weight function dependent on both position, $\boldsymbol{r}$, and wind speed $V(\boldsymbol{r}, t)$ and

A is the area of the blade.

Equation (1) can be simplified by considering the two following points:

1) The aerodynamic torque appears linear in the hub distance as the driving force on the blades is almost constant along the blade. [3]
2) The time scale of change in the wind field at low frequencies is similar or larger than the period of revolution of the rotor, and at any instant the contribution of the low frequency components to the torque is related to wind-field over the complete rotor disc.

Figure 4-1, [3], supports statement 1, which demonstrates the variation with distance from the hub of the force due to a blade element. Below 6m the driving force varies with position but the contribution of this section of blade to the total torque,T_A , is comparatively small. It follows that

$$T_A(t) \cong \int_{Ar} w\big(V(\boldsymbol{r}, t)\big) dA \tag{2}$$

Where $w\big(V(\boldsymbol{r}, t)\big)$ is some weight function dependent only on the wind speed and

Ar is the area swept by the rotor.

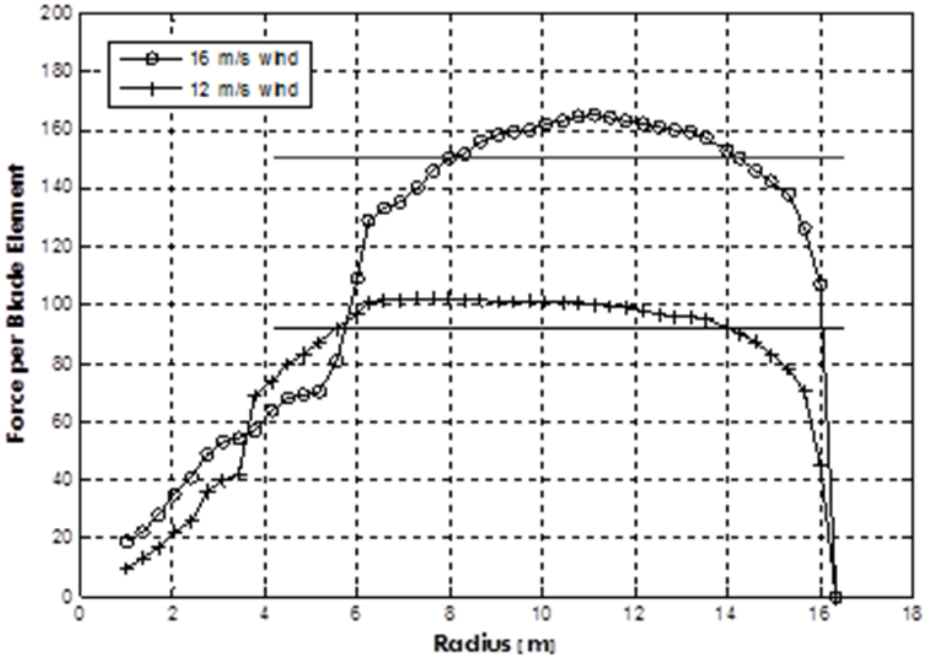

Figure 4-1: Force per unit blade element

As only the perturbation in the wind-field about the quasi-static mean needs to be considered, equation (2) can be simplified further.

As demonstrated in the following equation, the torque transient,$T(t)$, can be obtained by linearising equation (2) about the quasi-static mean wind speed such that

$$T(t) \cong k \int_{Ar} v(\boldsymbol{r}, t) dA \tag{3}$$

$v(\boldsymbol{r}, t)$ is the field of turbulent perturbations in the wind speed about the quasi-static mean perpendicular to the rotor disc and k is a normalising constant.

The auto-correlation function for the torque transient is

$$\begin{aligned} R_T(t) &= \int_{-\infty}^{\infty} T(s)T(t+s)ds \\ &\approx k^2 \int_{Ar} \int_{Ar} \int_{-\infty}^{\infty} v(\boldsymbol{r}_1, s)v(\boldsymbol{r}_2, t+s)ds dA_1 dA_2 \\ &= k^2 \int_{Ar} \int_{Ar} R_{v(\boldsymbol{r}_1)v(\boldsymbol{r}_2)}(t) dA_1 dA_2 \end{aligned} \tag{4}$$

Where the cross-correlation function between the wind at $\boldsymbol{r}_1$ and the wind at $\boldsymbol{r}_2$is represented by $R_{v(\boldsymbol{r}_1)v(\boldsymbol{r}_2)}$.

The following equation provides the relation of the spectrum of T, $S_T(\omega)$, to the cross-spectrum for the turbulent wind fluctuations, $S_{v(\boldsymbol{r}_1)v(\boldsymbol{r}_2)}$.

$$S_T(\omega) \cong k^2 \int_{Ar} \int_{Ar} S_{v(\boldsymbol{r}_1)v(\boldsymbol{r}_2)}(\omega) dA_1 dA_2 \quad (5)$$

The following equation is obtained on assumption that the spectrum of wind speed fluctuations at a fixed point is not related to position on the rotor disc

$$S_T(\omega) \cong k^2 S_v(\omega) \int_{Ar} \int_{Ar} X(\boldsymbol{r}_1, \boldsymbol{r}_2, \omega) dA_1 dA_2 \quad (6)$$

Where $S_v(\omega)$ is spectrum of wind speed fluctuation at a fixed point and

$$X(\boldsymbol{r}_1, \boldsymbol{r}_2, \omega) = \frac{S_{v(\boldsymbol{r}_1)v(\boldsymbol{r}_2)}(\omega)}{\sqrt{S_{v(\boldsymbol{r}_1)v(\boldsymbol{r}_2)}(\omega) S_{v(\boldsymbol{r}_1)v(\boldsymbol{r}_2)}(\omega)}} \quad (7)$$

The correlation of the wind speeds at the two points, $\boldsymbol{r}_1$ and $\boldsymbol{r}_2$, is mainly determined by their separation distance

$$l = \sqrt{\boldsymbol{r}_1^2 + \boldsymbol{r}_2^2 - 2\boldsymbol{r}_1.\boldsymbol{r}_2} \quad (8)$$

Hence, the coherence function for the wind from [4] can be assumed to be of the form

$$X(\boldsymbol{r}_1, \boldsymbol{r}_2, w) \cong \exp\left(\frac{-\gamma l w}{\bar{V}}\right) \quad (9)$$

Where γ is the turbulent wind speed decay factor and $\bar{V}$ is the mean wind speed.

It should be noted here that the quasi-static mean wind speed used on linearising (2) is not essentially the same as the mean wind speed,$\bar{V}$, since they may be averaged over different time intervals. However, the assumption here is that, $\bar{V}$ and the quasi-static mean wind speed is identical with γ accounting for the difference between two values.

A simple form for the spectrum of the aerodynamic torque transients is therefore obtained from

$$S_T(\omega) \cong k^2 S_V(\omega) \int_{Ar} \int_{Ar} exp\left(\frac{-\gamma l \omega}{\bar{V}}\right) dA_1 dA_2$$

$$= k^2 S_V(\omega) \phi(\chi) \quad (10)$$

where

$$\chi = \left(\frac{\gamma R}{\bar{V}}\right) \omega = \sigma\omega$$

and

$$\phi(\chi) = R^4 \int_D \int_D \exp(-\chi \bar{l})\, d\bar{A}_1 d\bar{A}_2$$

$$= 4\pi R^4 \int_0^1 s ds \int_0^{\pi} d\emptyset \int_0^{Scos\emptyset + \sqrt{1-s^2 sin^2\emptyset}} \bar{l} e^{-x\bar{l}} d\bar{l} \tag{11}$$

$$= \frac{2\pi^2 R^4}{x^2} - \frac{4\pi R^4}{x^2} \int_0^2 \sqrt{\frac{1-u^2}{4(1+xu)e^{-xu}}}\, du$$

$$= \frac{2\pi^2 R^4}{x^2} \left\{ 1 + \frac{4}{\pi} \int_0^{\frac{\pi}{2}} (1 - 3sin^2\theta) e^{-2xcos\theta} d\theta \right\}$$

Where R is the rotor radius and D is the disc with unit radius.

Hence,

$$\phi(\chi) \cong \pi^2 R^4 \frac{(2+x^2)}{(2+ax^2)\left(1+\frac{x^2}{a}\right)} \quad ; \quad a = 0.55 \tag{12}$$

That is

$$S_T(\omega) \cong k^2 R^4 \pi^2 S_V(\omega) \frac{(2+x^2)}{(2+ax^2)\left(1+\frac{x^2}{a}\right)} \tag{13}$$

Perturbations in an effective wind speed uniform over the rotor disc causes perturbations in the torque. The spectrum of the effective wind speed, $S(\omega)$, is obtained from

$$S(\omega) = \frac{(2+x^2)}{(2+ax^2)\left(1+\frac{x^2}{a}\right)} S_V(\omega) \tag{14}$$

Where $S_V(\omega)$ is the point wind speed. The fluctuation in point wind speed can be represented by spectra of the form

$$S_V(\omega) = \frac{\mathrm{K_v}|\omega|^{\mathrm{k}}}{[1+(\omega \mathrm{T_v})^{\alpha}]^{\delta}}$$

The factors such as surface roughness, turbulence intensity and the mean wind speed effect the constants $\mathrm{K_v}$ and $\mathrm{T_v}$. The turbulent spectrum used determines the parameters α, δ and k. Von Karman, Davenport, Dryden and Kaimal spectra are the most frequently used. However, the most appropriate spectra for point wind speed time series of a few minutes duration could be the Von Karman spectrum, which is as follow:

$$S_{Vk}(\omega) = 0.475\sigma_v^2 \frac{(\frac{L}{\hat{V}})}{(1+(\frac{\omega L}{\hat{V}})^2)^{5/6}}$$

where σ_v is the wind speed standard deviation,$\hat{V}$ is the mean wind speed, L is the turbulence length scale.

The spectrum,$S(\omega)$, can be normalised as follow

$$S(0) = S_V(0) \tag{15}$$

This is as a result of the very low frequency component of the turbulent fluctuations in the wind speed being uniform over the rotor disc.

By spectrally factorising the spectrum, $S(w)$, the linear model relating perturbations in torque to perturbations in point wind speed can be obtained, as demonstrated in Figure 4-2.

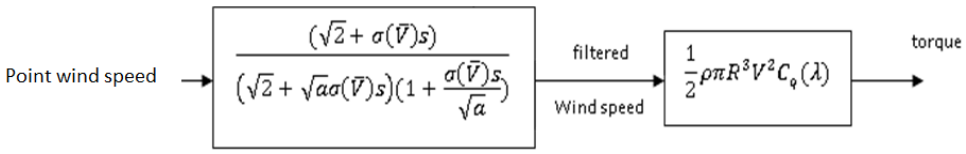

Figure 4-2: Linear model of torque perturbations

The following transfer function is used in Figure 4-2 to model the rotational averaging of wind speed.

$$f(s) = \frac{(\sqrt{2}+\sigma s)}{(\sqrt{2}+\sqrt{a}\sigma s)(1+\frac{\sigma s}{\sqrt{a}})} \tag{16}$$

To estimate the axial hub torque generated by the blade the nonlinear torque coefficients can be used in combination with the output from the filter (16), as demonstrated in Figure 4-3:

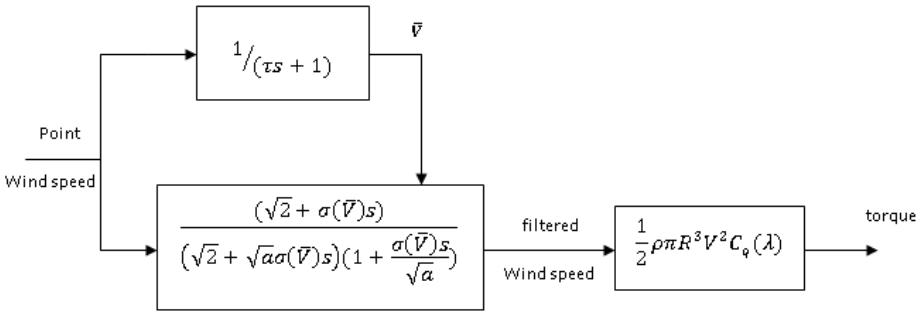

Figure 4-3: Nonlinear model of torque

As shown in Figure 4-3 the total wind speed, which includes the quasi-static mean is the input to the spatial filter. The following equation defines the relationship between wind speed and torque.

$$T = \frac{1}{2}\rho\pi R^3V^2C_q(\lambda) \tag{17}$$

where λ is the tip speed ratio $\lambda = \frac{\Omega R}{V}$, ρ is the density of air 1.225 kg/m^2, R is the radius of the rotor, V is the wind speed and Ω is the angular velocity of rotor.

The torque coefficient,$C_q(\lambda)$, is specific to the turbine of interest.

The purpose of using the filter $\frac{1}{(\tau s+1)}$ in the wind speed/rotor interaction model, Figure 4-3, is to average the wind speed over τ seconds. τ can be chosen appropriately to be equivalent to a few rotations of the rotor. The model can be expected to be valid for frequencies below $1\Omega_0$.

4.2. Dynamics of HAWT

The overall dynamic of a grid connected constant speed horizontal axis wind turbine consists of structural and drive train dynamics. The motions of blades, tower, etc. from structural dynamics affects the fatigue life of turbine. The drive-train dynamics affect the drive-train components such as the gearbox, and if the turbine is pitch regulated its control system would also be involved.

The combination of structural, drive-train, generator, and when appropriate, control system dynamics, determine the performance of a wind turbine. Despite the fact that the drive-train dynamics of a wind turbine are a combination of all different dynamic modes of the tower, blades, hub, low-speed shaft, gearbox, gear train, high-speed shaft and generator rotor, a simple model can approximate very closely to the drive-train dynamics for almost all wind turbines.

The equations of motion of the drive-train are represented in following sections. For more details, see [7].

4.2.1. Equation of motion of rotor

The two main structural modes of each blade, flap-wise and edge-wise, are considered in the direction of the principal axes of the blade. Both contribute directly to the drive-train dynamics. The position of the edge-wise mode plane is slightly tilted to the pitch plane and the flap-wise mode plane is perpendicular to the edge-wise mode plane. There are three dynamic modes of the rotor, formed by a combination of the dominant edge-wise modes of the three blades. Three modes consist of one blade stationary with the other two blades oscillating at the same frequency but exactly out of phase. The addition of these three oscillatory motions is zero as only two are independent. The other mode consists of all three blades oscillating in phase at the same frequency. Only the last mode transmits low frequency transient loads to the drive-train. Therefore, it is the only mode that needs to be considered here. Also, when considering the flap-wise rotor mode, there is only one mode that needs to be taken into accounts which is when all three blades oscillating in phase at the same frequency. As a result, the rotor can be represented by a single blade. The inertia of this single blade model of the rotor for the edge-wise mode can be estimated by the inertia of the complete rotor about the axis of the low-speed shaft. The stiffness should be approximated such that the frequency is the same as the natural frequency of a blade in an inertial reference frame, as shown below:

$$\omega^2 = \frac{K}{J}$$

K is the stiffness, J is the inertia and ω^2 should be same as the natural frequency of a blade in an inertial reference frame.

The radius of gyration for the flap wise mode and edge wise mode of a blade are approximately the same. Hence similar to the edge wise mode the inertia of the single blade model of the rotor for the flap wise mode can be estimated by the inertia of the complete rotor and stiffness should be approximated such that the frequency is the same as the natural frequency of a blade in an inertial reference frame.

The net effect of the side to side motion of the tower on the rotor aerodynamic forces is negligible. The tip speed of the blades increases/decreases with respect to its position relative to the hub, if it is higher than the hub the tip speed is increased (decreased) by the motion of the tower head and if the blade is lower than the hub the tip speed is decreased (increased). Also, the displacement of the blade in the plane of the rotor does not cause motion, relative to the tower head, of the centre of mass of the rotor for the dominant rotor mode. Therefore, the dynamics of the side to side motion of the tower is not required to be included in the analysis. However, the fore and aft motion of the tower influences the rotor aerodynamic forces and motion, relative to the tower head, of the centre of mass of the rotor. Therefore, the fore and aft motion of the tower couples directly to the rotor and should be accounted for.

The single blade model of the rotor is shown in Figure 4-4:

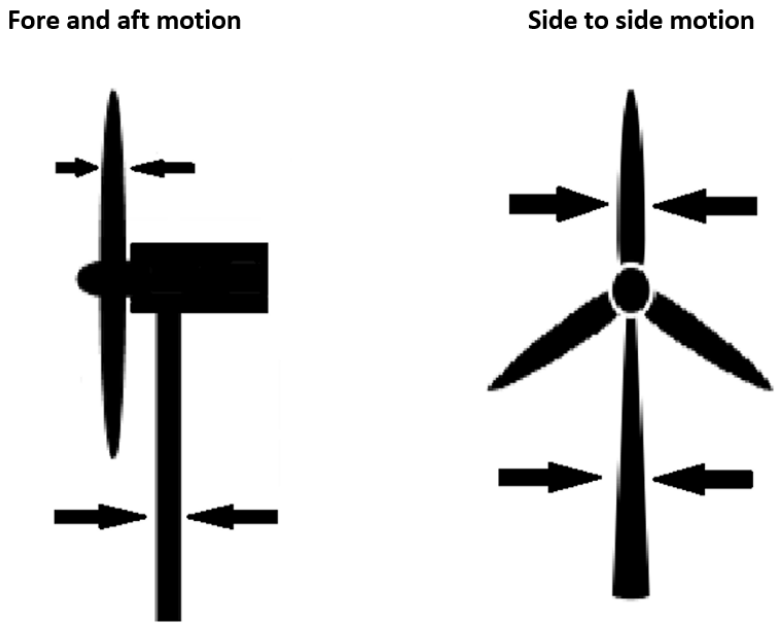

Figure 4-4: Single blade model

The Lagrangian for the system is:

$$L_R = \frac{1}{2}J\dot{\theta}_R^2 + \frac{1}{2}J\dot{\emptyset}_R^2 + \frac{1}{2}J_T\dot{\emptyset}_T^2 + J_C\dot{\emptyset}_R\dot{\emptyset}_T - \frac{1}{2}K_E[(\theta_R - \theta_H)\cos\beta - (\emptyset_R - \emptyset_T)\sin\beta]^2 - \frac{1}{2}K_F[(\emptyset_R - \emptyset_H)\sin\beta + (\emptyset_R - \emptyset_T)\cos\beta]^2 - \frac{1}{2}K_T\emptyset_T^2 + D_T\emptyset_T + F_1\theta_R + F_2\emptyset_R - \frac{1}{2}J\Omega_0^2(\emptyset_R - \emptyset_H)^2 - \frac{1}{2}J\Omega_0^2(\emptyset_R - \emptyset_T)^2 \quad (18)$$

Where J is the inertia of the rotor, θ_R is in-plane angular displacement of the centre of mass of the blade, $\emptyset_R$ is out-of-plane angular displacement of the centre of mass of the blade, θ_H is hub angular displacement, $\emptyset_T$ is fore-and-aft angular displacement of the hub, α is pitch angle of the blade, K_E and K_F are the edge wise and flap wise stiffnesses, F_1 and F_2 are the inplane and out of plane aerodynamic torques on the blade, Ω_0 is the nominal angular velocity of the rotor and β is the angle between the plane of the edge wise mode of the blade and plane of the rotor.

The centrifugal stiffening of the rotor is represented by the last two terms in equation (18). As discussed previously the dominant for and aft structural mode of the tower has been included in (18). J_T represents the total moment of inertia of the complete rotor and $J_C$is the tower/rotor cross coupling inertia

$$J_C = MhR_C$$

Where M is mass of the rotor, h is the hub height of the rotor and R_C is the distance from the hub to the centre of mass of a blade

The stiffness of the tower required to make the frequency equal to that of the fore and aft structural mode of the tower is represneted by K_T with the for and aft damping force represented by D_T such that

$$D_T = -B_T\dot{\emptyset}_T$$

(F_1/V^2) and (F_2/V^2) are in general functions of the tip speed ratio, λ, with

$$\lambda = R\Omega/V \quad ; \quad V = (w - h\dot{\emptyset}_T - L\dot{\emptyset}_R) \quad ; \quad \Omega = \dot{\theta}_R$$

Where R is radius of rotor, w is wind speed and $L\dot{\emptyset}_R$ is mean velocity of the blade relative to the wind speed.

The equations of motion of the rotor, (19), are:

$$J\ddot{\theta}_R = -(K_E + J\Omega_0^2)[(\theta_R - \theta_H)cos\beta - (\emptyset_R - \emptyset_T)sin\beta]cos\beta - (K_F + J\Omega_0^2)[(\theta_R - \theta_H)sin\beta + (\emptyset_R - \emptyset_T)cos\beta]sin\beta + F_1 \quad (19)$$

$$\frac{\left(1-\frac{J_C^2}{JJ_T}\right)}{\left(1+\frac{J_C}{J_T}\right)}J\ddot{\emptyset}_R = (K_E + J\Omega_0^2)[(\theta_R - \theta_H)\cos\beta - (\emptyset_R - \emptyset_T)\sin\beta]\sin\beta - (K_F + J\Omega_0^2)[(\theta_R - \theta_H)\sin\beta + (\emptyset_R - \emptyset_T)\cos\beta]\cos\beta + \left[F_2 - \frac{J_C}{J_T}D_T + \frac{J_C}{J_T}K_T\emptyset_T\right]/\left(1+\frac{J_C}{J_T}\right) \quad (20)$$

$$\frac{\left(1-\frac{J_C^2}{JJ_T}\right)}{\left(1+\frac{J_C}{J}\right)}J_T\ddot{\emptyset}_R = -(K_E + J\Omega_0^2)[(\theta_R - \theta_H)\cos\beta - (\emptyset_R - \emptyset_T)\sin\beta]\sin\beta + (K_F + J\Omega_0^2)[(\theta_R - \theta_H)\sin\beta + (\emptyset_R - \emptyset_T)\cos\beta]\cos\beta + \left[D_T - K_T\emptyset_T - \frac{J_C}{J}F_2\right]/\left(1+\frac{J_C}{J}\right) \quad (21)$$

The toque transmitted to the hub, T_H, is

$$T_H = (K_E + J\Omega_0^2)[(\theta_R - \theta_H)\cos\beta - (\emptyset_R - \emptyset_T)\sin\beta]\cos\beta - (K_F + J\Omega_0^2)[(\theta_R - \theta_H)\sin\beta + (\emptyset_R - \emptyset_T)\cos\beta]\sin\beta \quad (22)$$

The Lagrangian can be applied to rotors with any number of blades. However, equations (19-21) are derived assuming the rotor has three blades.

4.2.2. Simplification of rotor dynamics

Tower damping, D_T, is very small and can be neglected. With β constant, fore and aft angular displacement of the hub, $\emptyset_T$, can be determined from

$$\emptyset_T = \frac{J}{J_T}\frac{\left(1-\frac{J_C^2}{JJ_T}\right)}{\left(1+\frac{J_C}{J_T}\right)}\frac{(\omega_E^2-\omega_F^2)sin\beta cos\beta s^4}{\Delta}\theta_H - \frac{J}{J_T}\frac{\left(1-\frac{J_C^2}{JJ_T}\right)}{\left(1+\frac{J_C}{J_T}\right)}\frac{(\omega_E^2-\omega_F^2)sin\beta cos\beta s^2}{\Delta}\left(\frac{F_1}{J}\right)$$
$$+\frac{J}{J_T}\frac{\left(1-\frac{J_C^2}{JJ_T}\right)}{\left(1+\frac{J_C}{J_T}\right)\left(1+\frac{J}{J_T}\right)}\frac{(s^2(\omega_E^2 sin^2\beta+\omega_F^2 cos^2\beta)+\omega_E^2\omega_F^2)}{\Delta}\left(\frac{F_2}{J}\right) \quad (23)$$
$$-\frac{J_C}{J_T}\frac{\left(1-\frac{J_C^2}{JJ_T}\right)}{\left(1+\frac{J_C}{J_T}\right)\left(1+\frac{J}{J_T}\right)}\frac{s^2(s^2+\omega_E^2 cos^2\beta+\omega_F^2 sin^2\beta)}{\Delta}\left(\frac{F_2}{J}\right)$$

where *s* is the Laplace operator and

$$\omega_E^2 = \frac{K_E+J\Omega_0^2}{J} \quad ; \quad \omega_F^2 = \frac{K_F+J\Omega_0^2}{J} \quad ; \quad \omega_T^2 = \frac{K_T}{J_T}$$

and

$$\Delta = \left(\frac{1}{1+\frac{J_C}{J}}\right)\left[\left(1-\frac{J_C^2}{JJ_T}\right)s^2+\omega_T^2\right](s^2+\omega_E^2)(s^2+\omega_F^2)$$

$$+\frac{J}{J_T}\frac{1}{\left(1+\frac{J_C}{J}\right)}[(\omega_E^2 sin^2\beta+\omega_F^2 cos^2\beta)s^2+\omega_E^2\omega_F^2]\left[\left(1-\frac{J_C^2}{JJ_T}\right)s^2+\omega_T^2\frac{J_C}{J_T}\right] \quad (24)$$

$$-\frac{J_C}{J_T}\frac{1}{\left(1+\frac{J_C}{J_T}\right)}\left[\left(1-\frac{J_C^2}{JJ_T}\right)s^2+\omega_T^2\right]s^2(s^2+\omega_E^2 cos^2\beta+\omega_F^2 sin^2\beta)$$

It follows that the contribution of θ_H, F_1 and F_2 to equation (19) and (20) through $\emptyset_T$ is negligible as the inertia of the rotor is significantly less than the inertia of the complete turbine, i.e.

$$\frac{J}{J_T} \ll 1 \text{ and } \frac{J_C}{J_T} \ll 1$$

Therefore, the dynamics of the rotor can be represented by the following equations which ignore the dynamics of the tower:

$$\begin{bmatrix}\ddot{\theta}_R\\ \ddot{\emptyset}_R\end{bmatrix} = A(\beta)\begin{bmatrix}(\theta_R-\theta_H)\\ \emptyset_R\end{bmatrix}+\begin{bmatrix}\frac{F_1}{J}\\ \frac{F_2}{J}\end{bmatrix} \quad (25)$$

with

$$A(\beta) = -\begin{bmatrix}(\omega_E^2 cos^2\beta+\omega_F^2 sin^2\beta) & -(\omega_E^2-\omega_F^2)sin\beta cos\beta\\ -(\omega_E^2-\omega_F^2)sin\beta cos\beta & (\omega_E^2 sin^2\beta+\omega_F^2 cos^2\beta)\end{bmatrix} \quad (26)$$

and

$$\lambda = \frac{R\Omega}{v} \quad ; \quad v = w - L\dot{\emptyset}_R \quad ; \quad \Omega = \dot{\theta}_R \quad (27)$$

The hub torque (T_H) is:

$$T_H = J\omega_E^2[(\theta_R-\theta_H)cos\beta-\emptyset_R sin\beta]cos\beta+J\omega_F^2[(\theta_R-\theta_H)sin\beta+\emptyset_R cos\beta]sin\beta \quad (28)$$

4.2.3. Linearisation of rotor dynamics

Linearising equations (25) and (28) about an equilibrium point:

$$\theta_R = \Omega_0 t+\theta_{R_0}; \quad \theta_H = \Omega_0 t; \quad \emptyset_R = \emptyset_{R_0}; \quad w = w_0$$

such that

$$\begin{bmatrix}\theta_{R_0}\\ \emptyset_{R_0}\end{bmatrix} = \frac{A^{-1}(\beta)}{J}\begin{bmatrix}\frac{1}{2}w_0\frac{\partial F_1}{\partial w}+\frac{1}{2}\Omega_0\frac{\partial F_1}{\partial \Omega}\\ \frac{1}{2}w_0\frac{\partial F_2}{\partial w}+\frac{1}{2}\Omega_0\frac{\partial F_2}{\partial \Omega}\end{bmatrix} \quad (29)$$

and

$$\lambda_0 = \frac{R\Omega_0}{w_0}$$

There are three cases, stall regulation, part span regulation and full span regulation. They should be considered separately and here we only consider the full span regulation.

4.2.4. Full span regulation

Equations (25) to (28) are linearised such that

$$\theta_R = \Omega_0 t + \theta_{R_0} + \Delta\theta_R; \qquad \theta_H = \Omega_0 t + \Delta\theta_H; \qquad \emptyset_R = \emptyset_{R_0} + \Delta\emptyset_R; \qquad w = w_0 + \Delta w \tag{30}$$

The angle β changes according to the pitch angle as follow

$$\beta = \beta_E + \alpha \approx \alpha \tag{31}$$

where β_E is the angle between the plane of the pitch of a blade and the plane of its edge wise mode.

The aerodynamic torques, F_1 and F_2 are now dependent on pitch angle,α, as well as to λ and v. Pitch angle,α, can be represented by:

$$\alpha = \alpha_0 + \Delta\alpha \tag{32}$$

On linearising (25) to (28) with (30), (31) and (32) the equations of motion can be approximated by:

$$\begin{bmatrix} \left(s^2 - \frac{s\frac{\partial F_1}{\partial \Omega}}{J} + \omega_E^2 cos^2\alpha_0 + \omega_F^2 sin^2\alpha_0\right) & \left(\frac{sL\frac{\partial F_1}{\partial w}}{J} - (\omega_E^2 - \omega_F^2) sin\alpha_0 cos\alpha_0\right) \\ \left(-\frac{s\frac{\partial F_2}{\partial \Omega}}{J}\right) - (\omega_E^2 - \omega_F^2) sin\alpha_0 cos\alpha_0 & \left(s^2 + \frac{sL\frac{\partial F_2}{\partial w}}{J} + \omega_E^2 cos^2\alpha_0 + \omega_F^2 sin^2\alpha_0\right) \end{bmatrix} \begin{bmatrix} \Delta\theta_R \\ \Delta\emptyset_R \end{bmatrix}$$

$$= \begin{bmatrix} (\omega_E^2 cos^2\alpha_0 + \omega_F^2 sin^2\alpha_0) & \frac{\frac{\partial F_1}{\partial w}}{J} & \frac{F_{1\alpha}}{J} \\ -(\omega_E^2 - \omega_F^2) sin\alpha_0 cos\alpha_0 & \frac{\frac{\partial F_2}{\partial w}}{J} & \frac{F_{2\alpha}}{J} \end{bmatrix} \begin{bmatrix} \Delta\theta_H \\ \Delta w \\ \Delta\alpha \end{bmatrix} \tag{33}$$

where

$$F_{1\alpha} = \frac{\partial F_1}{\partial \alpha} + \frac{(w_E^2 - w_F^2)}{2w_E^2 w_F^2}\left[(w_E^2 + w_F^2) sin\alpha_0 cos\alpha_0 \left(w_0 \frac{\partial F_1}{\partial w} + \Omega_0 \frac{\partial F_1}{\partial \Omega}\right) + (w_E^2 cos^2\alpha_0 - w_F^2 sin^2\alpha_0)(w_0 \frac{\partial F_2}{\partial w} + \Omega_0 \frac{\partial F_2}{\partial \Omega})\right] \tag{34}$$

$$F_{2\alpha} = \frac{\partial F_2}{\partial \alpha} + \frac{(w_E^2 - w_F^2)}{2w_E^2 w_F^2}\left[(w_E^2 sin^2\alpha_0 - w_F^2 cos^2\alpha_0)\left(w_0 \frac{\partial F_1}{\partial w} + \Omega_0 \frac{\partial F_1}{\partial \Omega}\right) + (w_E^2 + w_F^2) sin\alpha_0 cos\alpha_0 (w_0 \frac{\partial F_2}{\partial w} + \Omega_0 \frac{\partial F_2}{\partial \Omega})\right] \quad (35)$$

The rotor dynamics can now be represented by the model illustrated in Figure 4-5:

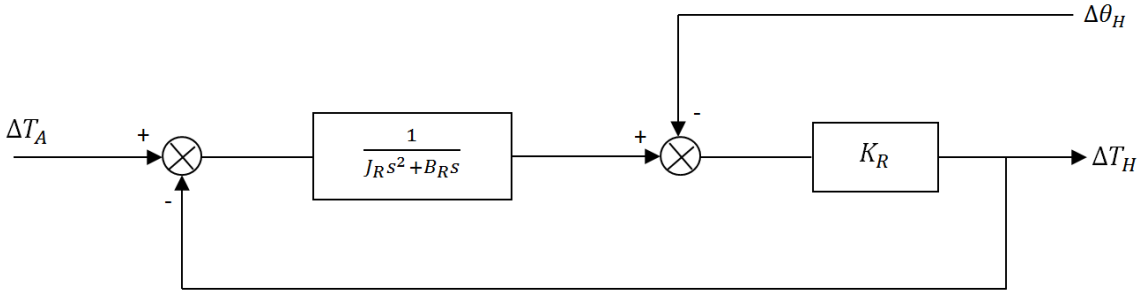

Figure 4-5: Canonical form of dynamics of the rotor

where

$$J_R = \frac{J(\omega_E^2 cos^2\alpha_0 + \omega_F^2 sin^2\alpha_0)}{\omega_E^2}$$

and K_R is defined by

$$K_R = J_R \omega_E^2$$

and B_R is defined by

$$B_R = \left[-cos^2\alpha_0 \frac{\partial F_1}{\partial w} + Lsin\alpha_0 cos\alpha_0 + Lsin^2\alpha_0 \frac{\partial F_2}{\partial w} + sin\alpha_0 cos\alpha_0 \frac{\partial F_2}{\partial \Omega}\right] \cdot \frac{(\omega_E^2 cos^2\alpha_0 + \omega_F^2 sin^2\alpha_0)}{\omega_E^2} \quad (36)$$

at low frequencies

$$B_R = \frac{\partial F_1}{\partial \Omega}(\omega_E^2 cos^2\alpha_0 + \omega_F^2 sin^2\alpha_0)/\omega_E^2 \quad (37)$$

The relationship of $\Delta\theta_H$ and ΔT_H defines the contribution of the rotor to the drive train dynamics. This relationship can be modelled by figure 4.5 for all types of regulation. This model is an inertia with damping attached to the hub by a massless spring. Any differences in comparison to the original model (19) to (22), is local to the natural frequency of the tower,ω_T, and the edge wise and flap wise natural frequencies of the blade, $\omega_E$and $\omega_F$respectively.

4.3. Rotor and hub dynamics

In the previous section the rotor dynamics is described by a simple spring mass damper model. The model is extended in this chapter to include the hub.

From the previous section the simplified linear equations of motions for the rotor, which are brought forward to this section are

$$J_R\ddot{\theta}_R = -B_R\dot{\theta}_R + T_A - T_H \quad ; \quad T_H = K_R(\theta_R - \theta_H) \tag{38}$$

4.3.1. Equation of motion of hub

The low speed shaft must also be considered when analysing the rotor dynamics including the hub. The low speed shaft can be considered massless by distributing part of its inertia to the inertia of the hub and part to the inertia of the first stage of the gearbox as the inertia of the low speed shaft is a lot less than the inertia of either of them. This distribution is split evenly when the low speed shaft is uniform. The system is shown in Figure 4-6.

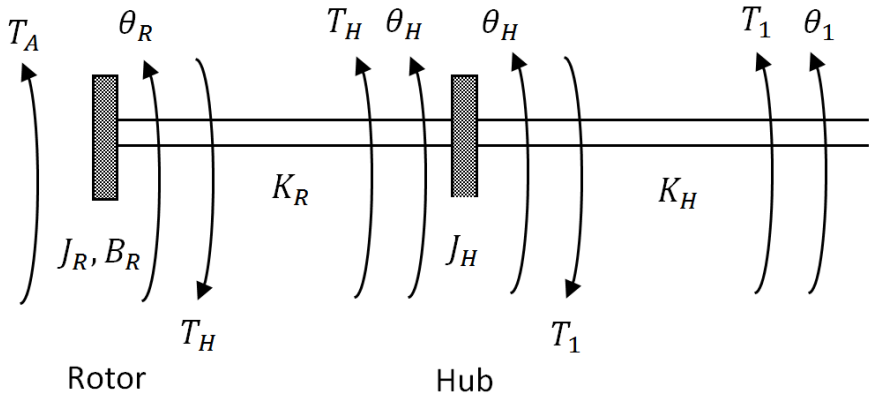

Figure 4-6: The rotor, hub and low speed shaft

The equations of motion of the hub are:

$$J_H\ddot{\theta}_H = T_1 - T_H \quad ; \quad T_1 = K_H(\theta_H - \theta_1) \tag{39}$$

4.3.2. Simplification of the rotor and hub dynamics

The dynamics of the rotor, hub and low speed shaft is represented by the block diagram shown in Figure 4-7.

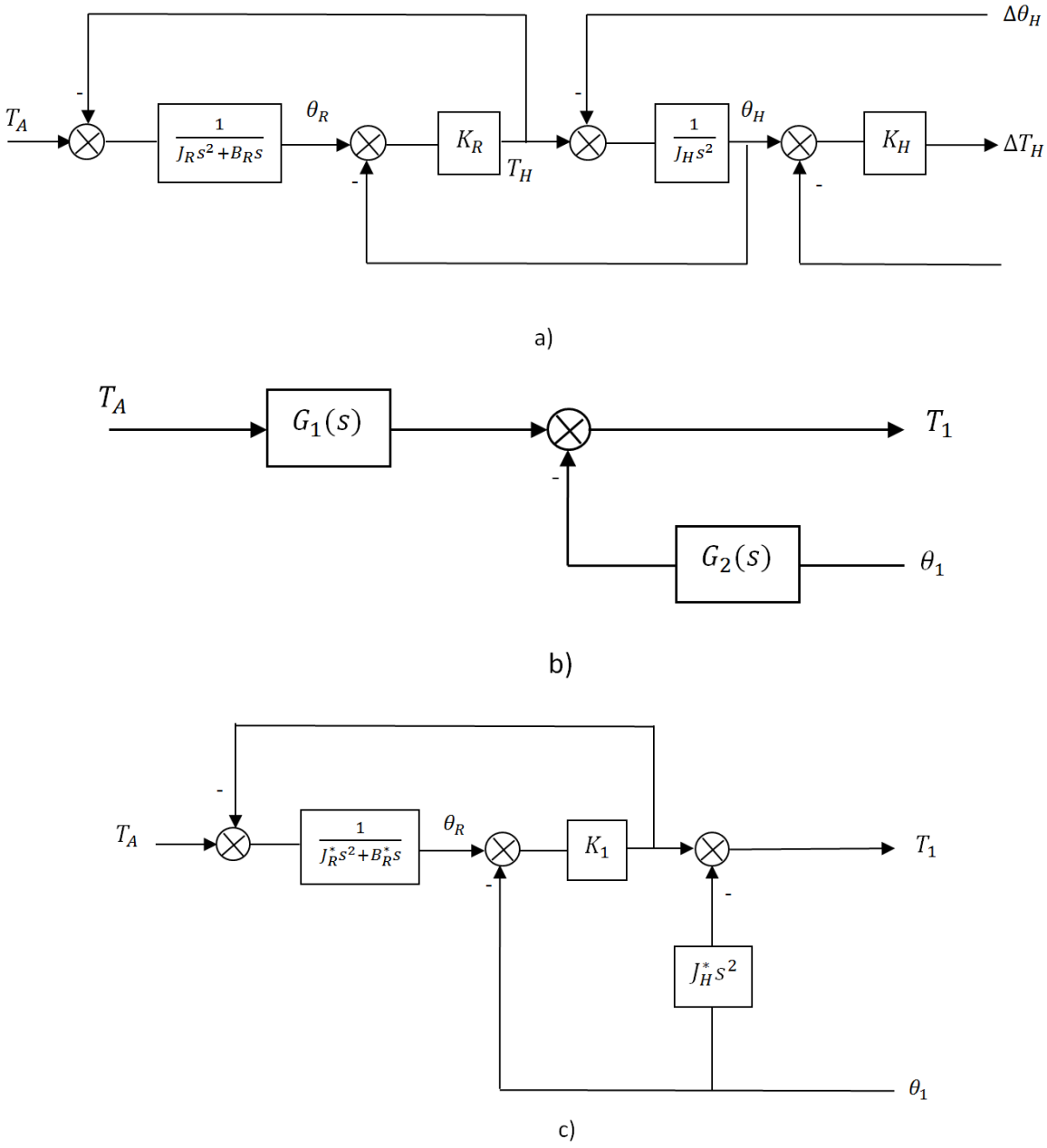

Figure 4-7: The dynamics of the rotor, hub and low speed shaft

Figure 4-7 (a) is equivalent to Figure 4-7 (b) when

$$G_1(s) = \frac{K_R K_H}{D(s)} \tag{40}$$

and

$$G_2(s) = \frac{K_H[J_H J_R s^4 + J_H B_R s^3 + (J_H + J_R)K_R s^2 + B_R K_R s]}{D(s)} \tag{41}$$

The denominator of (40) and (41),$D(s)$, is

$$D(s) = [J_H J_R s^4 + J_H B_R s^3 + \big((K_R + K_H)J_R + K_R J_H\big)s^2 + (K_R + K_H)B_R s + K_R K_H]$$

Which has the two dynamic mode form

$$D(s) = J_H J_R[s^2 + \alpha_1 s + \beta_1][s^2 + \alpha_2 s + \beta_2] \quad (42)$$

B_R can be set to zero, when determining β_1 and β_2, as the damping is too small to noticeably shift the magnitude of the roots of the equation (42). It follows that

$$\beta_1 = \frac{(K_R(J_H+J_R)+K_H J_R)-\mu\sqrt{1+4J_H^2 K_H K_R^3/((K_R+K_H)^2\mu^2)}}{2J_R J_H}$$

where

$$\mu = \frac{[J_R(K_R+K_H)^2+J_H K_R(K_R-K_H)]}{(K_R+K_H)}$$

β_1 can also be approximated by the following equation when $\frac{K_R}{K_H} \ll 1$ or $\frac{K_H}{K_R} \ll 1$ or $\frac{J_H}{J_R} \ll 1$

($\frac{J_H}{J_R} = \frac{1}{10}$ is definitely small enough and even $\frac{J_H}{J_R} = \frac{1}{6}$ would be small enough)

$$\beta_1 \approx \frac{\frac{K_R K_H}{J_R(K_R+K_H)}}{[1+\frac{J_H}{J_R}\frac{K_R^2}{(K_R+K_H)^2}][1-\frac{(J_H/J_R)^2 K_R^3 K_H/(K_R+K_H)^4}{1+(J_H/J_R)K_R(K_R-K_H)/(K_R+K_H)^2}]}$$

$$\approx \frac{\frac{K_R K_H}{J_R(K_R+K_H)}}{[1+\frac{J_H}{J_R}\frac{K_R^2}{(K_R+K_H)^2}]}$$

As K_R and/or K_H tend to infinity, this approximation would be exact. Similarly,

$$\beta_2 = \frac{(K_R(J_H+J_R)+K_H J_R)-\mu\sqrt{1+4J_H^2 K_H K_R^3/((K_R+K_H)^2\mu^2)}}{2J_R J_H}$$

$$\approx \frac{\frac{(K_R+K_H)}{J_H}}{[1+\frac{J_H}{J_R}\frac{K_R^2}{(K_R+K_H)^2}]}$$

The damping coefficient, $\alpha_1$and α_2 are

$$\alpha_1 \approx \frac{\frac{B_R}{J_R}}{[1+\frac{J_H}{J_R}\frac{K_R^2}{(K_R+K_H)^2}]}$$

$$\alpha_2 \approx \frac{\frac{B_R}{J_R}\frac{J_H}{J_R}\frac{K_R^2}{(K_R+K_H)^2}}{[1+\frac{J_H}{J_R}\frac{K_R^2}{(K_R+K_H)^2}]}$$

The damping ratio of the second factor in (42) is

$$\eta_2 = \frac{\alpha_2}{2\sqrt{\beta_2}} \approx \eta_R \left(\frac{J_H}{J_R}\right)^{\frac{3}{2}} \left(\frac{K_R}{(K_R+K_H)}\right)^{5/2} \tag{43}$$

where

$$\eta_R = \frac{B_R}{2\sqrt{K_R J_R}}$$

is the damping factor of the rotor. η_2 is a lot less than one and the effect of the second factor in equation (42) on phase is limited to the vicinity of the frequency, $\beta_2^{\frac{1}{2}}$. Also, the following ratio of the squares of the two frequencies is small.

$$\frac{\beta_1}{\beta_2} \approx \frac{J_H}{J_R} \frac{K_R K_H}{(K_R+K_H)^2} \tag{44}$$

The contribution of the second factor in the equation defining $D(s)$ to the backward path drive train dynamics, which relates T_1 to θ_1, can be considered as not significant due to the separation between the two frequencies, as indicated by equation (44), the low level of damping at higher frequency, as indicated by equation (43), and also to the presence of further compliance in the drive train, sufficient to roll off the gain to less than 0 dB. However, the contribution of this factor to the forward path, which relates *T* to T_A , would remain significant. Therefore, $D(s)$ can be approximated by

$$D(s) \approx J_H J_R [s^2 + \alpha_1 s + \beta_1] \beta_2 \tag{45}$$

Provided the factor $\frac{(s^2+\alpha_2 s+\beta_2)}{\beta_2}$ is absorbed within $T_w(s)$ and, when required, $T_\alpha(s)$. Hence

$$G_2(s) \approx \frac{K_H s[s+B_R/(J_R+J_H)][s^2+\alpha_3 s+\beta_3]}{\beta_2[s^2+\alpha_1 s+\beta_1]} \tag{46}$$

with

$$\alpha_3 \approx \frac{B_R J_H}{J_R(J_R+J_H)} ; \qquad \beta_3 \approx \frac{K_R(J_R+J_H)}{J_H J_R} \tag{47}$$

In the numerator of the equation (46) the damping factor for the quadratic term is

$$\eta_3 = \frac{\alpha_3}{2\sqrt{\beta_3}} \approx \eta_R \left(\frac{J_H}{(J_H+J_R)}\right)^{3/2} \tag{48}$$

Compared to other sources of damping in the drive train, the damping terms of the order of $(B_R J_H / J_R)$ can be considered negligible. Hence, figure 4.7 (c) is an equivalent representation of the rotor and hub dynamics, where

$$J_R^* = J_R(1 + J_H/J_R \frac{K_R}{(K_R+K_H)}) \quad ; \quad J_H^* = J_H \frac{K_H}{(K_R+K_H)}$$

$$B_R^* = B_R \quad ; \quad K_1 = \frac{K_R K_H}{(K_R+K_H)}(1 + \frac{K_R}{(K_R+K_H)} \frac{J_H}{J_R}) \tag{49}$$

Equation (49) is valid under the same conditions as relate to the factorisation of equation (42).

The inertia of the hub, J_H^*, can be considered as an additive term to the inertia of the first stage of the gearbox as the rotor can be understood as a single compliant blade attached by a massless shaft to the hub which in turn is attached rigidly to the gearbox.

4.4. Gearbox dynamics

The analysis of the gearbox presented in this section can be applied to a gearbox with any number of stages, however it is assumed the gearbox has three stages.

4.4.1. Equation of motion of gearbox

The gearbox is mounted on a damped compliant suspension as represented in Figure 4-8.

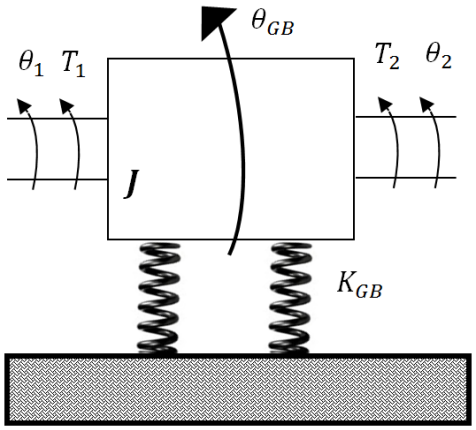

Figure 4-8: Gearbox system

$$J = \begin{bmatrix} J_{GG} & J_{GS} \\ J_{GS} & J_{SS} \end{bmatrix}$$

Torques T_1 and T_2 are positive when acting on gearbox.

In addition, motion relative to the tower head of the centre of mass of the gearbox is induced by the side to side motion of the tower. Therefore, the side to side motion of the tower couples directly to the gearbox, so it should be considered in the analysis.

Consider the gearbox rigidly mounted, the equations of motion are

$$J_s\ddot{\theta}_1 = T_1 + NT_2 \qquad ; \qquad \theta_2 = N\theta_1 \tag{50}$$

J_s is inertia of gear train reflected to the low speed shaft and N is gearbox ratio.

The gearbox ratio is positive if the rotation of the output shaft is in the same direction as the input and is negative when rotation is opposite. The dynamics are by the block diagram in Figure 4-9.

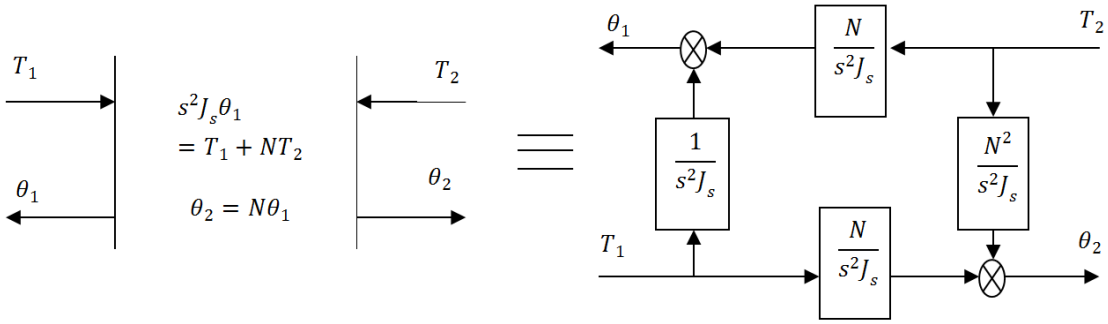

Figure 4-9: Block diagram representation of rigidly mounted gearbox

Considering the gearbox is mounted on a compliant suspension, the dynamics are related to the three angular displacements, θ_1, θ_2 and θ_{GB} as well as the angular displacement, θ_T, of the tower. However, there are only two degrees of freedom since

$$\theta_2 = N\theta_1 - (N-1)\theta_{GB} \tag{51}$$

Figure 4-10 demonstrates the arrangement of the gear train. It should be noted that the gear ratios, N_1, N_2 and N_3 also follow the same sign convention as applies to the gearbox ratio.

$$N = N_1N_2N_3 \tag{52}$$

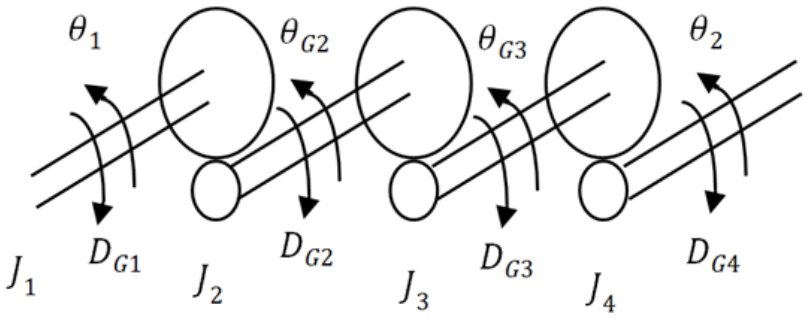

$$(\theta_{G2} - \theta_{GB}) = N_1(\theta_1 - \theta_{GB})$$

$$(\theta_{G3} - \theta_{GB}) = N_2(\theta_{G2} - \theta_{GB})$$

$$(\theta_2 - \theta_{GB}) = N_3(\theta_{G3} - \theta_{GB})$$

$$D_{G1} = -B_{GT1}\dot{\theta}_1$$

$$D_{G2} = -B_{GT2}\dot{\theta}_{G2}$$

$$D_{G3} = -B_{GT3}\dot{\theta}_{G3}$$

$$D_{G4} = -B_{GT4}\dot{\theta}_2$$

Figure 4-10: Schematic arrangement of gear train

The Lagrangian equation for the system is:

$$L_{GB} = \frac{1}{2}J_{GG}\dot{\theta}_{GB}^2 - J_{GS}\dot{\theta}_1\dot{\theta}_{GB} + \frac{1}{2}J_{SS}\dot{\theta}_1^2 + \frac{1}{2}J_T\dot{\theta}_T^2 + J_X\dot{\theta}_T\dot{\theta}_{GB} - \frac{1}{2}K_{GB}(\theta_{GB} - \theta_T)^2 - \frac{1}{2}K_T\theta_T^2 + T_1\theta_1 + T_2(N\theta_1 - (N-1)\theta_{GB}) + D_T\theta_T + D_{GB}\theta_{GB} + D_{GT1}\theta_1 + D_{GT2}\theta_{GB} \quad (53)$$

The inertia of the gear train reflected to the low speed shaft $J_S$is

$$J_S = J_1 + N_1^2J_2 + N_1^2N_2^2J_3 + N_1^2N_2^2N_3^2J_4$$

and the elements forming the gearbox inertia matrix, J, are

$$J_{GG} = J_{GB} + (N_1 - 1)^2J_2 + (N_1N_2 - 1)^2J_3 + (N_1N_2N_3 - 1)^2J_4$$

$$J_{GS} = N_1(N_1 - 1)J_2 + N_1N_2(N_1N_2 - 1)J_3 + N_1N_2N_3(N_1N_2N_3 - 1)J_4 \quad (54)$$

$$J_{SS} = J_S$$

The complete gear box inertia is represented by $J_{GB}$with the components of the gear train considered as point masses. The tower/gearbox cross coupling inertia is defined by J_x as follow

$$J_X = MhR_{GB}$$

R_{GB} is the distance from the axis of rotation of gearbox to its centre of mass.

D_{GT_1} and D_{GT_2} represent damping losses in the gear train as follow

$$D_{GT_1} = -B_{G_1}\dot{\theta}_1 - NB_{G_2}\dot{\theta}_2$$

and

$$D_{GT_2} = (N-1)B_{G_2}\dot{\theta}_2 - B_{G_3}\dot{\theta}_3$$

where

$$B_{G_1} = B_{GT_1} + \frac{N_1(N_1-1)}{N(N-1)}B_{GT_2} + \frac{N_1N_2(N_1N_2-1)}{N(N-1)}B_{GT_3} + B_{GT_4}$$

$$B_{G_2} = \frac{N_1(N_1-1)}{N(N-1)}B_{GT_2} + \frac{N_1N_2(N_1N_2-1)}{N(N-1)}B_{GT_3} + B_{GT_4}$$

$$B_{G_3} = -\frac{(N_1-1)(N-N_1)}{N}B_{GT_2} - \frac{(N_1-N_2-1)(N-N_1-N_2)}{N}B_{GT_3}$$

The gearbox mounting damping force is defined by D_{GB} as follow

$$D_{GB} = -B_{GB}\dot{\theta}_{GB}$$

The tower side to side damping force is defined by D_T as follow

$$D_T = -B_T\dot{\theta}_T$$

The tower is considered symmetric therefore for side to side and fore and aft motion the inertia, damping and stiffness are the same. However, by the differring cross coupling to the rotor and drive train the natural frequency of the side to side and fore and aft modes of the tower are split.

Follwing from the Lagrangian equation of the gearbox defined in equation (53) the equation of motion for the gearbox can be represented by:

$$J_{SS}\ddot{\theta}_1 - J_{GS}\ddot{\theta}_{GB} = T_1 + NT_2 - B_{G1}\dot{\theta}_1 - NB_{G2}\dot{\theta}_2 \tag{55}$$

$$\begin{aligned} &J_{GG}(1 - J_X^2/J_TJ_{GG})\ddot{\theta}_{GB} - J_{GS}\ddot{\theta}_1 \\ &= -K_{GB}(1 + J_X/J_T)(\theta_{GB} - \theta_T) \\ &+ K_T J_X/J_T\theta_T - (N-1)T_2 - (N-1)B_{G2}\dot{\theta}_2 - B_{G3}\dot{\theta}_{GB} - B_{GB}\dot{\theta}_{GB} + J_X/J_T B_T\dot{\theta}_T \end{aligned} \tag{56}$$

$$J_T\left(1 - \frac{J_{GS}^2}{J_{GG}J_{SS}} - \frac{J_X^2}{J_TJ_{SS}}\right)\ddot{\theta}_T = -K_{GB}(1 + \frac{J_S}{J_{GG}} - \frac{J_{GS}^2}{J_{GG}J_{SS}})(\theta_T - \theta_{GB})$$

$$-K_T\left(1-\frac{J_{GS}^2}{J_{GG}J_{SS}}\right)\theta_T+(N-1)\frac{J_x}{J_{GG}}T_2-\frac{J_xJ_{GS}}{J_{GG}J_{SS}}(T_1+\mathrm{N}T_2) \qquad (57)$$

$$-\frac{J_x}{J_{GG}}\left(D_{GB}+D_{GT_2}\right)+(1+\frac{J_{GS}^2}{J_{GG}J_{SS}})D_T-\frac{J_xJ_{GS}}{J_{GG}J_{SS}}\,D_{GT_1}$$

4.5. Drive train dynamics

The drive-train consists of the rotor, hub, low speed shaft, gearbox with damped compliant suspension, high speed shaft and generator rotor. The equation of motion of rotor, hub, low speed shaft and gearbox are explained in previous sections and the required equations are brought forward to this section.

4.5.1. Equations of motion of generator rotor

The inertia of the high-speed shaft can be considered massless as it is much less than either of the generator rotor inertia or the gear train inertia reflected to the high-speed shaft. If necessary, its inertia can be distributed, with appropriate fractions, to the inertia of the generator rotor and to the inertia of the final stage of the gearbox. When the high-speed shaft is uniform the inertia is distributed evenly.

It should be noted that difference in angular velocity between the two ends of shafts is small as they are stiff and considered massless. Therefore, two of the gearbox damping terms, $B_{G1}\dot{\theta}_1$ and $B_{G2}\dot{\theta}_2$, can be intepreted as amendments to the torques, T_1 and T_2. Also, these damping terms can be transferred to J_R^* and J_G, respectively, as they are light and the discrepancy at high frequency can be ignored.

The equations of motion for the generator rotor and high-speed shaft can be represented by the following equations:

$$J_G\ddot{\theta}_G=T_G-T_2 \qquad ; \qquad T_2=K_2(\theta_G-\theta_2) \qquad (58)$$

4.6. Induction generator dynamics

In order to complete the drive train model represented in previous sections a simple model of the induction generator is required.

This simple model can be represented by the first order linear differential equation, as shown below, and would be adequate for almost most cases, even for simulation based analysis.

$$\tau\dot{T}_G=-T_GD_e(\dot{\theta}_G-\dot{\theta}_e/p)$$

τ is the generator time constant

D_e is the slope of the torque/speed curve

p is number of pole pairs

$\dot{\theta}_e$ is the frequency of the grid

4.7. Complete drive train model

The combined dynamics of the drive-train can be represented by the model in Figure 4-11.

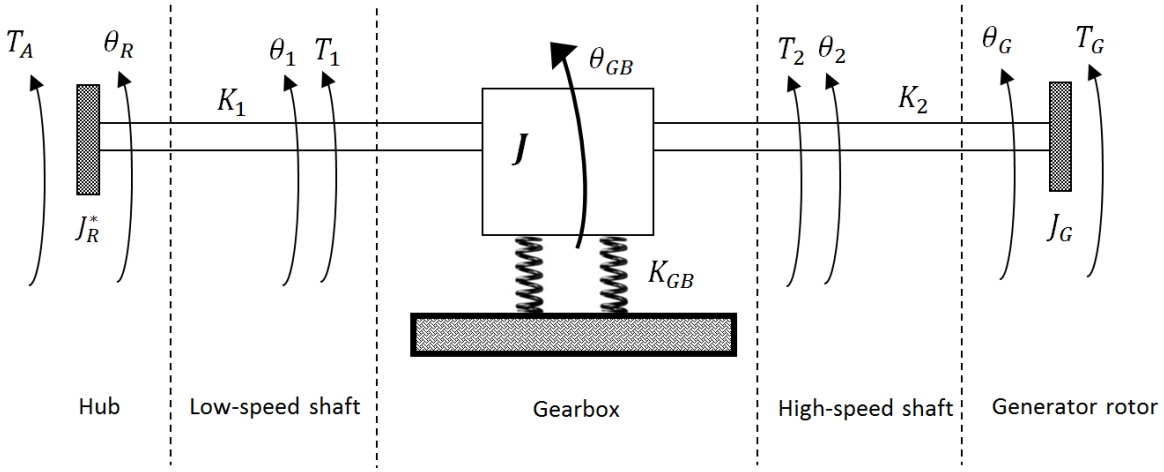

Figure 4-11: General drive train system

Torques T_A and T_G act on the inertia J_R^* and J_G respectively. Torques T_1 and T_2 act on gearbox.

As a conclusion all significant dynamics of the drive train including coupling to the tower can be modelled by equations (19),(20),(21),(22),(39),(52),(55),(56),(57) and (58).

4.8. Simple drive train model

The drive train dynamics is suitable for analysing the behaviour of the drive-train. To simulate the dynamic characteristic of the drive train a simpler model is required. The complexity of the detailed model makes the physical aspect difficult to understand even though it is more accurate.

Assuming that the gearbox is not compliantly mounted, the drive-train dynamic can be modelled by Figure 4-12 for almost all wind turbines, which would be more appropriate for the purpose of this thesis.

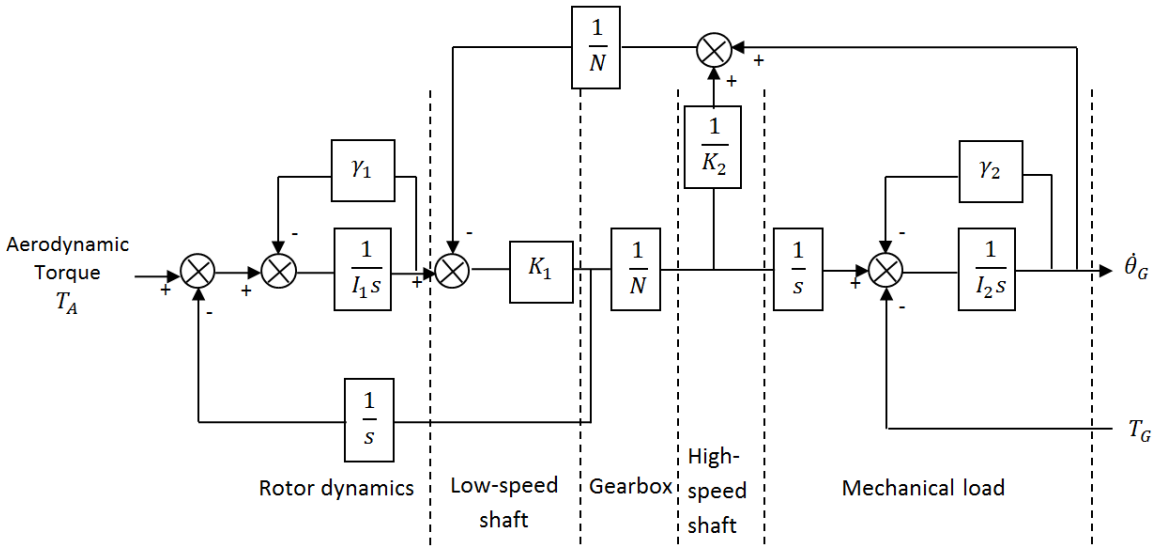

Figure 4-12: Drive train dynamics

T_G is Generator torque

$\dot{\theta}_G$ is Generator speed

I_1 is lumped rotor inertia

γ_1 is low speed shaft damping constant

K_1 is low speed shaft stiffness

I_2 is lumped generator rotor inertia

γ_2 is high speed shaft damping constant

K_2 is high speed shaft stiffness

N is gear ratio

5. Simulation of the mathematical model in Simulink

5.1. Wind model simulation

As explained in chapter 4.1, the axial hub torque generated by the blade can be estimated using the filtered wind speed output as input to a nonlinear torque coefficient.

The spatial filter brought forward from chapter 4.1, which is used for rotational averaging of the wind speed, is modelled by the following transfer function, f(s)

$$f(s) = \frac{(\sqrt{2}+\sigma s)}{(\sqrt{2}+\sqrt{a}\sigma s)(1+\frac{\sigma s}{\sqrt{a}})}$$

To simulate the above transfer function in Simulink, it is formulated in terms of integral equations as below: (note that σ is in function of mean wind speed $(\bar{v})$)

$$y = \frac{(\sqrt{2}+\sigma(\bar{v})s)}{(\sqrt{2}+\sqrt{a}\sigma(\bar{v})s)(1+\frac{\sigma(\bar{v})s}{\sqrt{a}})}$$

$$y = \frac{(\frac{\sigma(\bar{v})}{\sqrt{2}}+1)}{\frac{\sigma(\bar{v})^2}{\sqrt{2}}s^2+\left(\frac{\sigma(\bar{v})}{\sqrt{a}}+\frac{\sqrt{a}\sigma(\bar{v})}{\sqrt{2}}\right)s+1}$$

$$\frac{\sigma(\bar{v})^2}{\sqrt{2}}\ddot{y}\left(\frac{1}{\sqrt{a}}+\frac{\sqrt{a}}{\sqrt{2}}\right)\sigma(\bar{v})\dot{y}+y=\frac{1}{\sqrt{2}}\sigma(\bar{v})\dot{x}+x$$

$$\frac{\sigma(\bar{v})}{\sqrt{2}}(\sigma(\bar{v})\dot{y}-x)'=x-y-\left(\frac{1}{\sqrt{a}}+\frac{\sqrt{a}}{\sqrt{2}}\right)\sigma(\bar{v})\dot{y}$$

$$(\sigma(\bar{v})\dot{y}-x)=\int\frac{\sqrt{2}}{\sigma(\bar{v})}[x-y-\left(\frac{1}{\sqrt{a}}+\frac{\sqrt{a}}{\sqrt{2}}\right)\sigma(\bar{v})\dot{y}]dt$$

$$\dot{y}=\frac{x}{\sigma(\bar{v})}+\frac{1}{\sigma(\bar{v})}\int\sqrt{2}\,\sigma^{-1}(\bar{v})[x-y-\left(\frac{1}{\sqrt{a}}+\frac{\sqrt{a}}{\sqrt{2}}\right)\sigma(\bar{v})\dot{y}]dt$$

$$y=\int\{\frac{x}{\sigma(\bar{v})}+\sigma^{-1}(\bar{v})\int\sqrt{2}\,\sigma^{-1}(\bar{v})[x-y-\left(\frac{1}{\sqrt{a}}+\frac{\sqrt{a}}{\sqrt{2}}\right)\sigma(\bar{v})\dot{y}]\}dt$$

The integral equation representing the spatial filter is implemented in Simulink as shown in Figure 5-1:

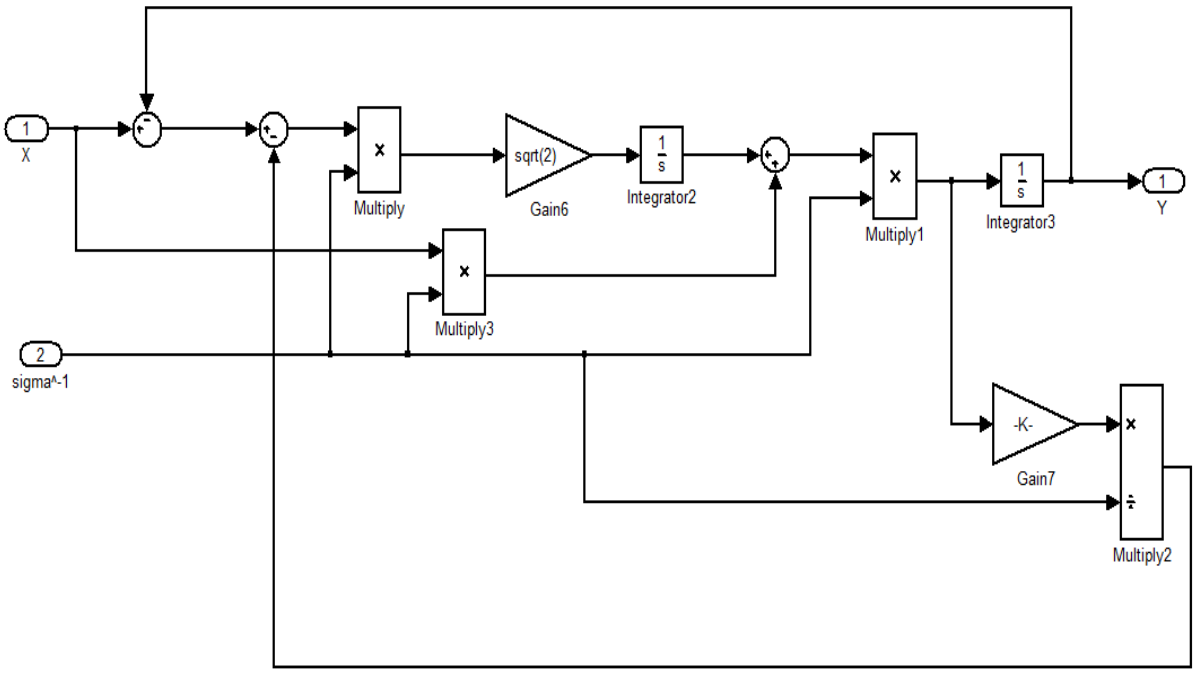

Figure 5-1: Spatial filter model in Simulink

σ (sigma) is function of mean wind speed and is calculated as shown below:

$$\sigma = \frac{\gamma R}{\bar{V}}$$

γ represents the turbulent wind speed decay factor and is set to 1.3 as recommended by Madsen and Frandsen [2].

R represents the radius of the rotor which interacts with the wind speed and $\bar{V}$ is the mean wind speed.

To simulate the mean wind speed,$\bar{V}$, a first order filter $\frac{1}{\tau s+1}$ is used to average the point wind speed over a sampling time, τ. The appropriate value to be chosen for τ should be equivalent to a few rotations by rotor; therefore, it was chosen to be 30s.

The input to the spatial filter is of course the point wind speed. The Dryden spectrum is used to represent the point wind speed fluctuation. It is a rational polynomial expression and can be modelled by

$$\dot{v}_d = -a_d v_d + b_d w$$

where v_d is wind speed, w is white Gaussian noise and v_d must be offset by $\hat{v}$ as it has zero mean. a_d and b_d are selected such that the Dryden spectrum is a best fit approximation [17] to the Von Karman spectrum, specifically

$$a_d = 1.14(\frac{\hat{V}}{L}) ; b_d = \sigma_v\sqrt{2a_d}$$

σ_v is the standard deviation of the wind speed, $\hat{V}$ is the mean wind speed and *L* is the turbulence length scale.

An appropriate value for *L* is 200m, which is for a wind turbine with a hub height of 30m.

The point wind speed and mean wind speed are implemented in Simulink as shown in Figure 5-2.

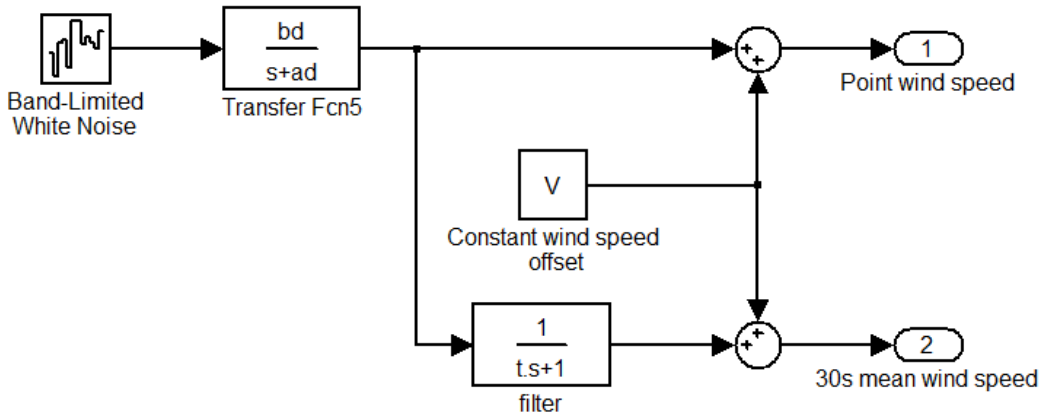

Figure 5-2: Point wind speed in Simulink

The simulation is for 610s (just over 10 minutes) with constant offset of 8m/s and 20% turbulence intensity. The graphs of point wind speed and 30s mean wind speed, are obtained from the model depicted in Figure 5-3, Figure 5-4 and Figure 5-5:

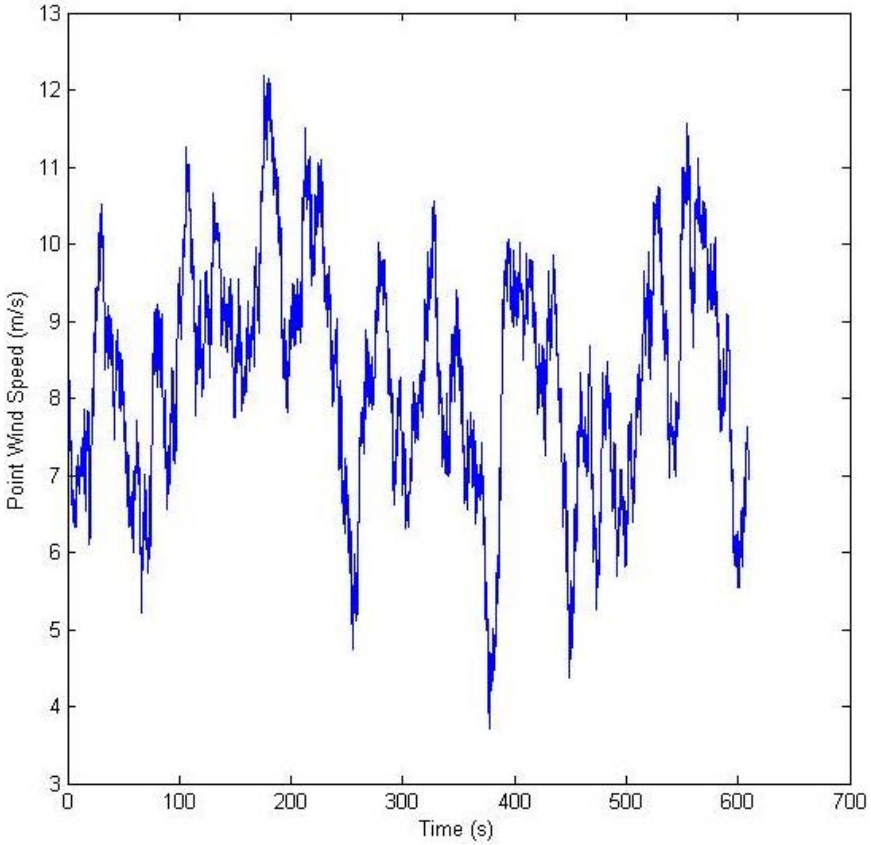

Figure 5-3: Point wind speed

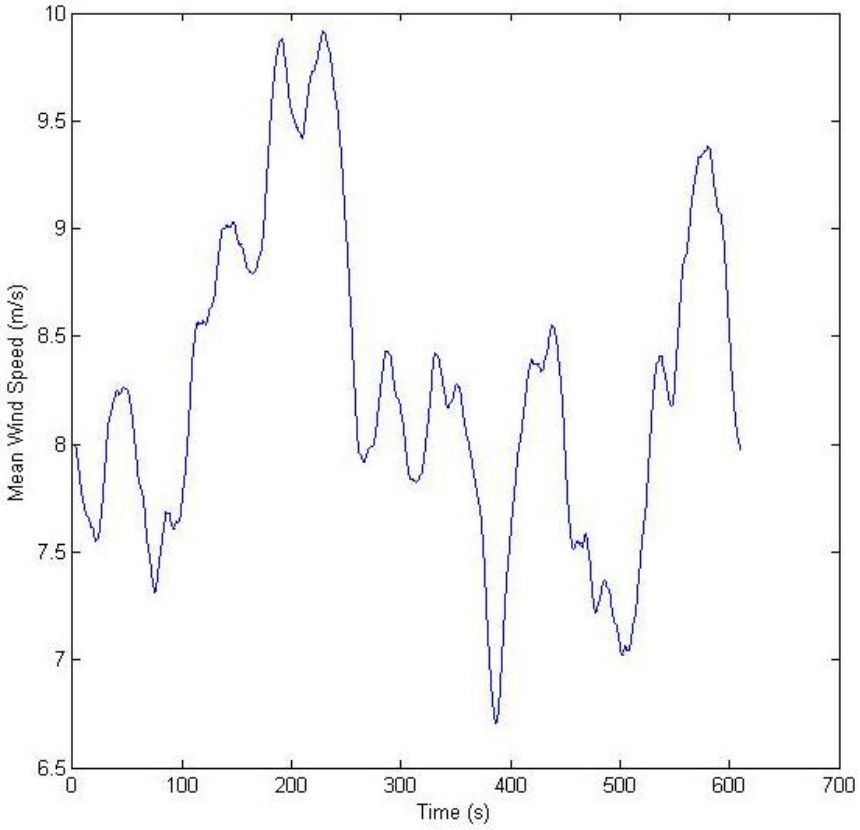

Figure 5-4: Mean wind speed

Feeding the point wind speed and the mean wind speed to the spatial filter model depicted in Figure 5-1 provides the filtered wind speed as shown in Figure 5-5:

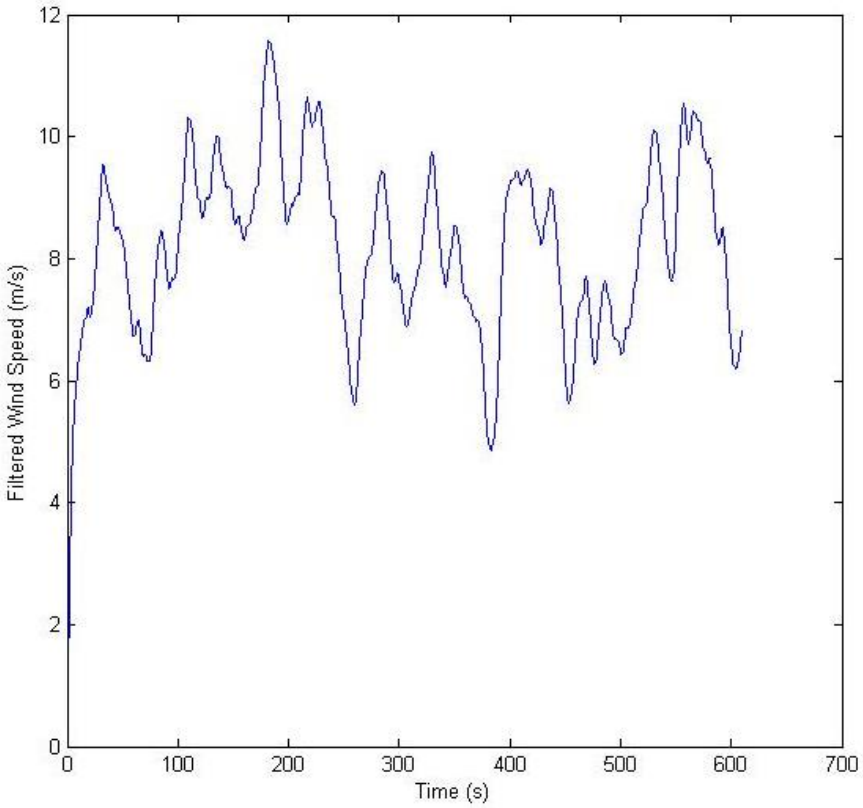

Figure 5-5: Filtered wind speed

As discussed in chapter 4.1, Figure 4-2, the filtered wind speed is input to the following equation to estimate aerodynamic torque:

$$T = \frac{1}{2}\rho\pi R^3 V^2 C_q(\lambda)$$

It should be noted that the torque coefficient,C_q, as a function of tip speed ratio, λ, is

$$C_q = \frac{C_p}{\lambda}$$

C_p is the power coefficient and

$$\lambda = \frac{\Omega R}{V}$$

where Ω is the rotor speed, R is the radius of the rotor and V is the wind speed

The power coefficient, C_p, is a function of the tip speed ratio and pitch angle. To calculate C_q, a look up table is used. The C_p look up table uses the C_p values of the 2MW Supergen exemplar wind

turbine. The table is given in Appendix B. The calculation of the pitch angle and the pitch actuator will be explained in section 6.4.2 . The equation relating wind speed to torque is implemented as shown in Figure 5-6.

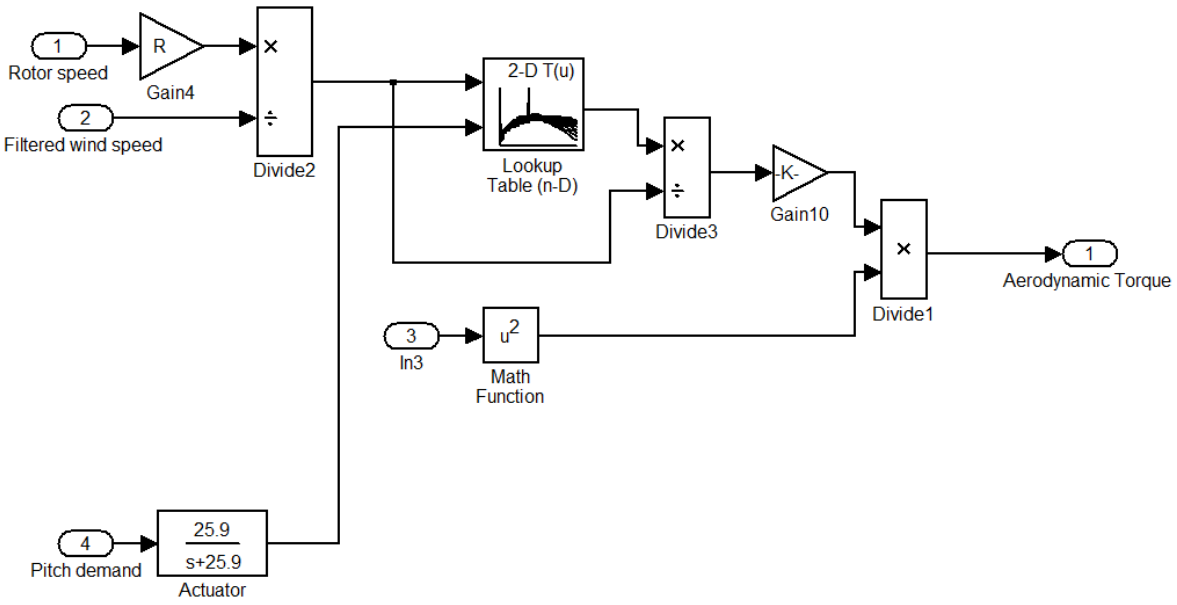

Figure 5-6: Aerodynamic torque calculation in Simulink

Where

$$K = \frac{1}{2}\rho\pi R^3$$

The point wind speed model, spatial filter and the equation relating the wind speed to torque were combined in Simulink as shown in Figure 5-7:

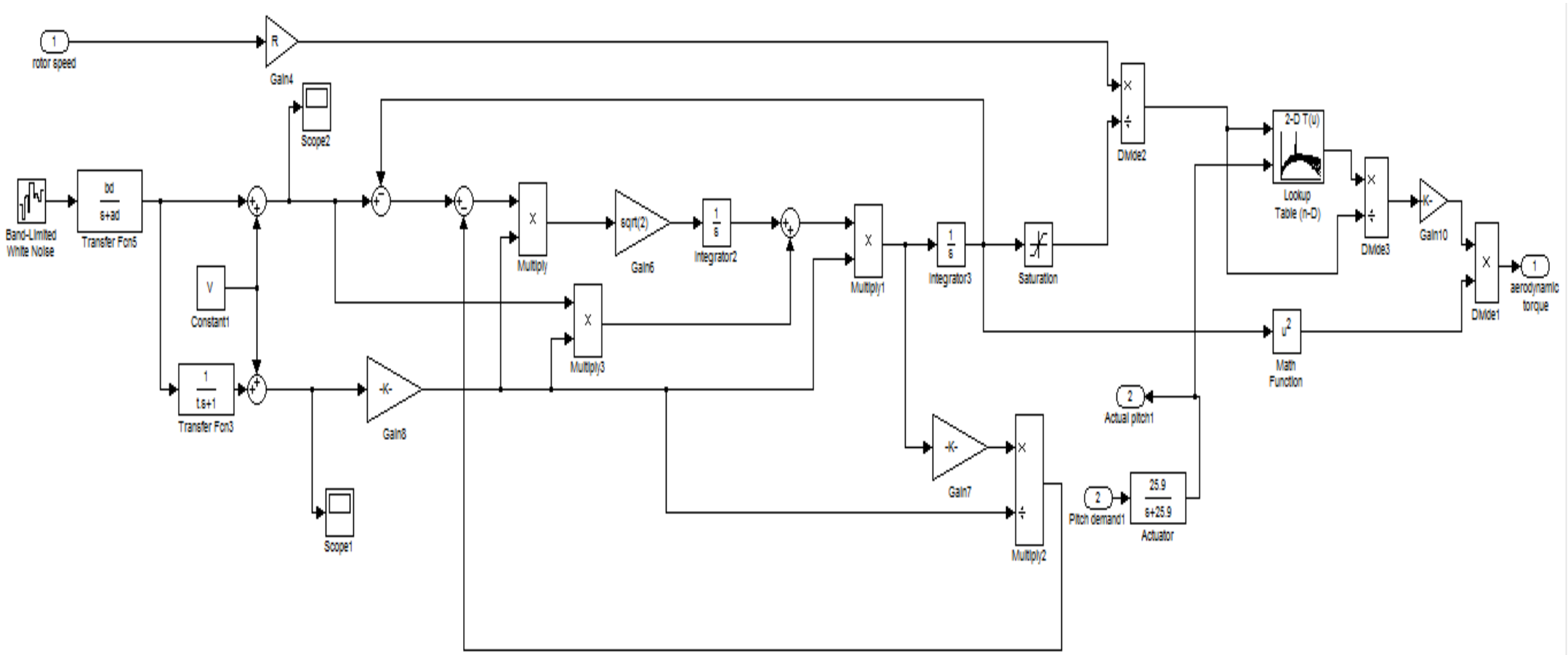

Figure 5-7: Wind model and torque calculation

5.2. Power train model simulation

Before implementing the drive train model described in Chapter 4 in Simulink, the algebraic loop in the model should be resolved. The section of the dynamics with an algebraic loop is that depicted in Figure 5-8:

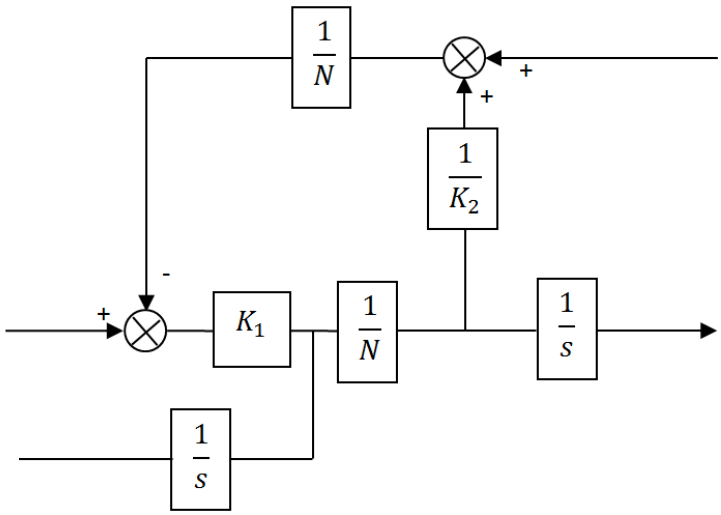

Figure 5-8: Algebraic loop in simulation

The algebraic loop is isolated in Figure 5-9:

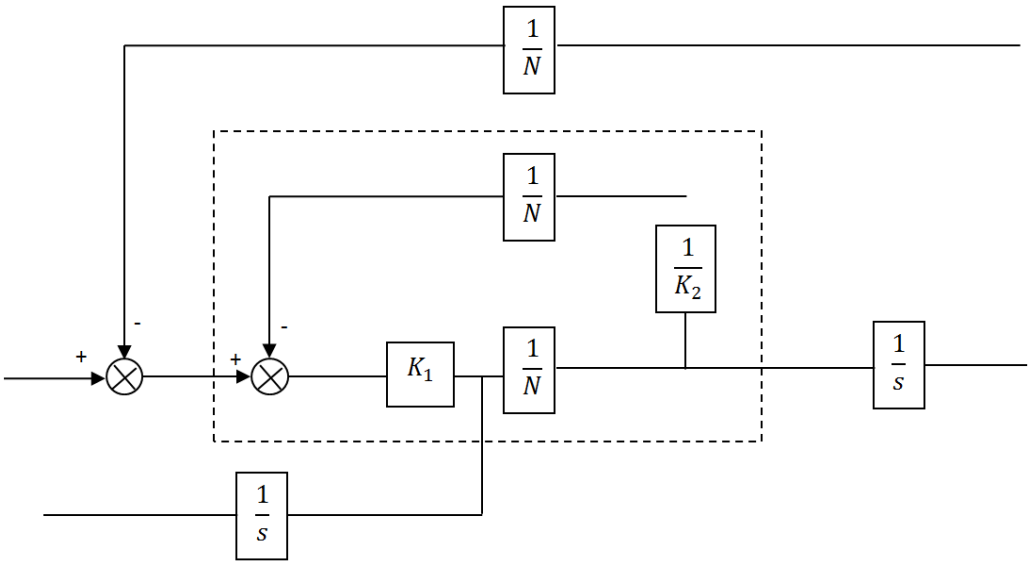

Figure 5-9: Isolating the algebraic loop in simulation

Now the algebraic loop, inside the dashed line in Figure 5.7, can be replaced by the gain G, in Figure 5-10:

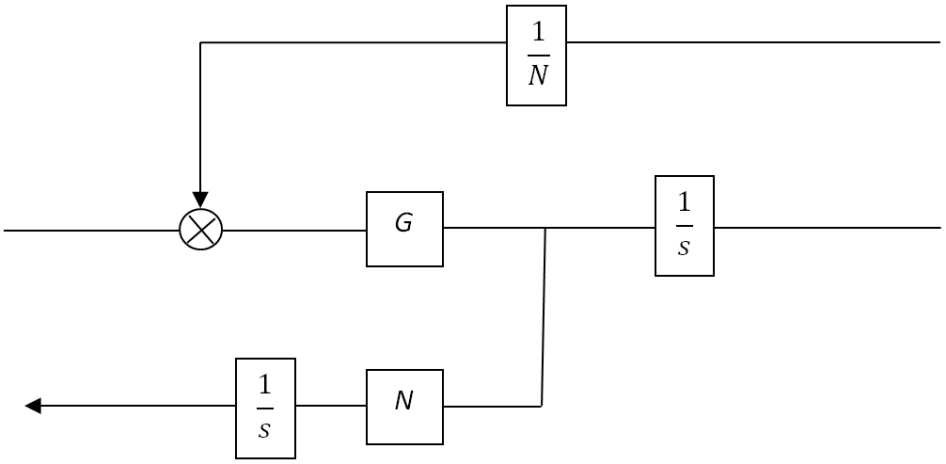

Figure 5-10: Replacing the algebraic loop by G

The gain, G, is calculated as follow. From the original block diagram, the following equation is obtained:

$$K_1\left(\frac{1}{N}\right)\left(x - y\left(\frac{1}{K_2} * \frac{1}{N}\right)\right) = y$$

which can be solved for y, as follows

$$\frac{K_1}{N}x - y\frac{K_1}{N}\left(\frac{1}{K_2} * \frac{1}{N}\right) = y$$

$$\frac{K_1}{N}x = y + y\frac{K_1}{N}\left(\frac{1}{K_2 N}\right)$$

$$\frac{K_1}{N}x = y + y\left(\frac{K_1}{K_2 N^2}\right)$$

$$\frac{K_1}{N}x = y\left(1 + \frac{K_1}{K_2 N^2}\right)$$

$$y = \frac{\frac{K_1}{N}}{1+\frac{K_1}{K_2 N^2}}\, x$$

Multiply top and bottom by $K_2 N^2$

$$y = \frac{N K_1 K_2}{N^2 K_2 + K_1}\, x \qquad ; \qquad G = \frac{N K_1 K_2}{N^2 K_2 + K_1}$$

After solving the algebraic loop, the drive train is implemented in Simulink as shown in Figure 5-11:

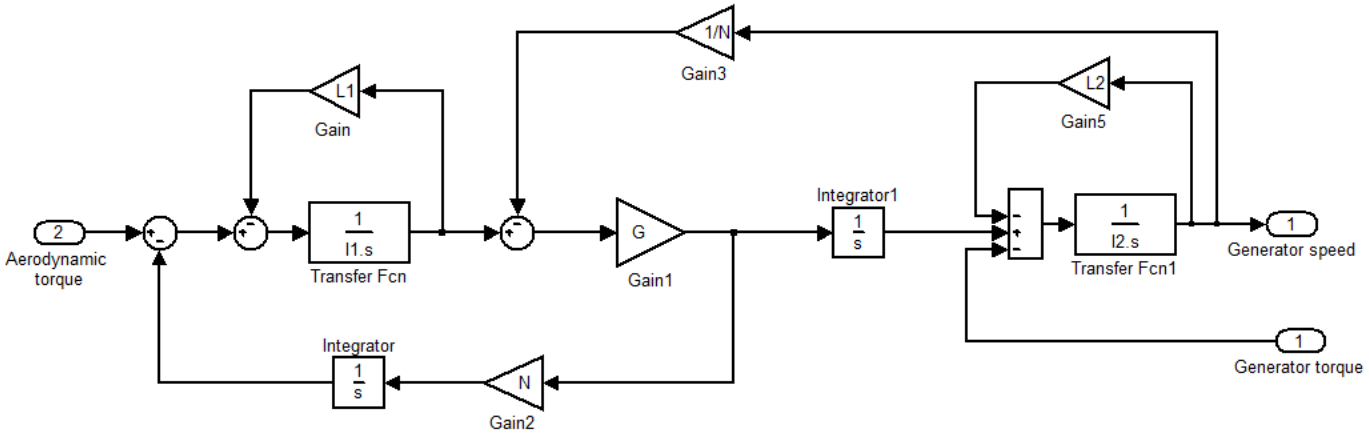

Figure 5-11: Drive train dynamics

As explained in chapter 4.6, a simple linear model for the generator dynamics with constant supply voltage is

$$\tau \dot{T}_G + T_G = D_e(\dot{\theta}_G - \frac{\dot{\theta}_e}{p})$$

$$T_G = \left(\frac{D_e}{1+s\tau}\right)(\dot{\theta}_G - \frac{\dot{\theta}_e}{p})$$

The generator dynamic model is implemented in Simulink as depicted in Figure 5.10:

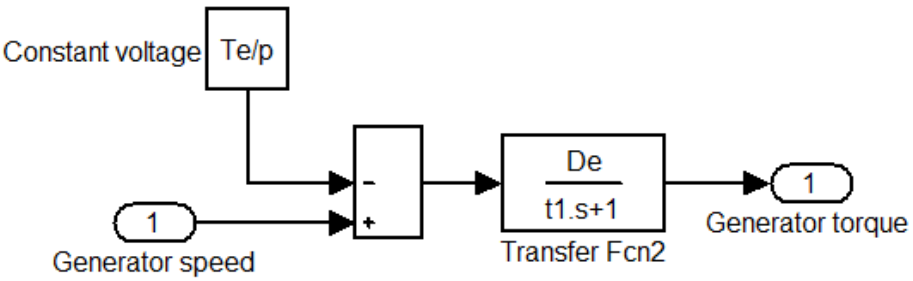

Figure 5-12: Generator dynamic model

The complete power train model is implemented by connecting the drive train model to the generator model. As demonstrated in Figure 5-12, the output of the generator model is generator torque which is input to the drive-train model shown in Figure 5-11.

6. Control System

6.1. Control system objectives

The performance of a control system can only be evaluated in terms of the criteria to which it is designed. Therefore, it is required to possess a clear statement of intent for the control system.

The general objectives of the control system are summarised as follow [22]:

1) Alleviating the transient loads throughout the wind turbines.
2) Regulating and smoothing the power
3) Ensuring that the power train has the appropriate dynamics, particularly damping of the power train.
4) Maximising the energy capture

The general goals stated above apply to designing a control system for both constant speed and variable speed wind turbine in full range of operation (below rated, rated and above rated). As this thesis is focused on operation of constant speed wind turbines in below rated region, the control system objective is only to maximise the energy capture. Unlike above rated region that the controller should pitch the blades to discard some of the energy in the wind to keep the energy capture at the rated value, the controller objective in below rated region is focused on extracting as much power as possible from the wind. It should be stated that the real purpose of the control system is to alleviate the structural load transients and thus the fatigue throughout the wind turbine to maximise its life. Alleviating these loads indirectly results in smooth power. The achievement of this particular control objective to reduce the structural load transients is a function of the choice of control strategy but not necessarily the combination of the related controller.

However, loads reduction is not discussed any further here, and the only objective focused on is the energy capture. Energy capture is dependent on both control strategy and the effectiveness of the related controller.

6.2. Control strategy

6.2.1. Definition of control strategy

Specifying the rotor speed as a function of wind speed is a reasonable method to define the control strategy that is in the context of rotor speed/wind speed plane. The operating points should be determined from the wind speed but as the direct measurement of wind speed experienced by the turbine is not possible, it should be estimated by measurements such as electrical power and rotor

speed which are made on the wind turbine itself. However, due to nonlinearity of the aerodynamics, there are some issues with this approach. As there is the possibility that more than one operating point could relate to a wind speed or more than one wind speed could relate to an operating point. Therefore, determining the operating point by just relying on knowledge of the wind speed is not valid.

An alternative context to the rotor speed/wind speed plane can be used to define the control strategy, namely, the torque/rotor speed plane [23, 24 and 25]. The control strategies can be defined with respect to either aerodynamic torque,T_f, drive train torque, T_D, or even a combination of the two. Therefore, there would be some uncertainties about the identity of the torque.

When the control strategy is defined with respect to the drive train torque,T_D, clarification is required as it could refer to torque at different points in the drive train, such as the low speed shaft torque or the generator reaction torque. Different torque can be used for different purposes. For example, to study the behaviour of the wind turbine in the torque/rotor speed plane the low speed shaft torque can be used. The most suitable torque for defining the controller would be the generator or reaction torque scaled by the gearbox ratio. The difference between the low speed shaft torque and generator reaction torque is the drive train losses.

Any control strategy defined in the torque/rotor speed is equivalent to a curve. The control system is then responsible to cause the turbine to track this curve.

In the torque/rotor speed context the knowledge of wind speed is no longer required, as the wind turbine operating point can be estimated by estimating the aerodynamic torque.

6.3. Control strategy options

In order to achieve maximum power output on a constant speed wind turbine in below rated region, the blades may have to be pitched slightly to vary the optimum angle of attack. Different strategy options are available for maximising the power capture for variable speed wind turbine, such as tracking the $C_p$max curve by using different reference points such as drive train torque or aerodynamic torque. In some special cases the general control strategies defined for variable speed wind turbines, where the main objective is defined to track the $C_p$max curve, can also be employed in constant speed wind turbines with altering the reference points. Since constant speed operation can be treated as a special case (operating region) in variable speed wind turbine.

As it can be observed from the variable speed operational strategy curve, depicted in Figure 6-1, there are two operational regions that the rotor speed is kept constant. However, these strategies are not discussed any further here.

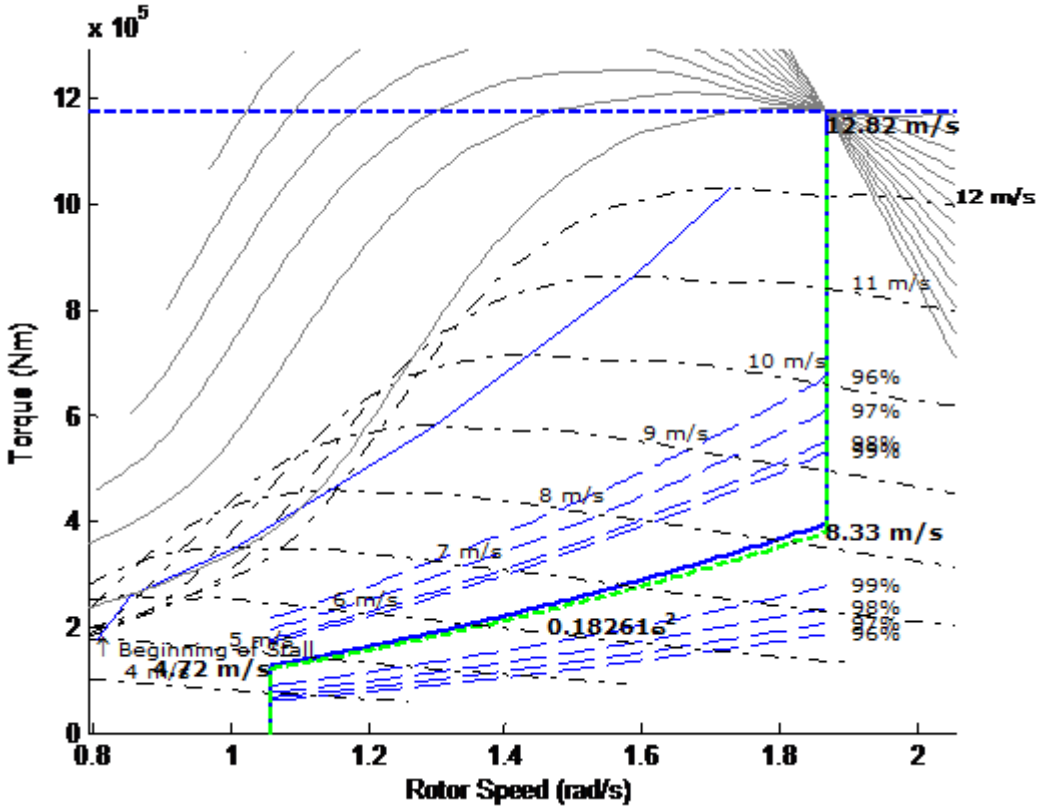

Figure 6-1: Operational strategy curve

6.3.1. Use of pitch angle to vary the angle of attack

The wind turbine blades are designed to generate a lift force due to their shape when swept through the wind field. The more curved side of the blade results in presence of low pressure air while the flatter side of the blade experiences high pressure air, therefore, generating lift force perpendicular to the direction of air flow as depicted in Figure 6-2:

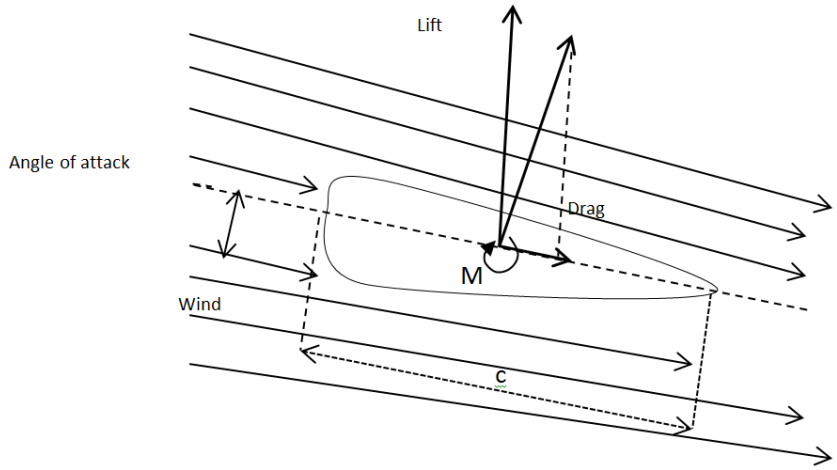

Figure 6-2: Angle of attack

As shown in Figure 6-2, apart from the lift force, the force in the flow is also decomposed into a force parallel to the direction of the flow which is referred to as drag. Lift and drag coefficients, C_l and C_d, are defined as:

$$C_l = \frac{L}{\frac{1}{2}\rho V^2 c} \qquad \text{and} \qquad C_d = \frac{LD}{\frac{1}{2}\rho V^2 c}$$

ρ is density

c is length of the aerofoil (chord)

It is also required to define the moment M about a point in the aerofoil, which is normally located on the chord line at $\frac{c}{4}$ from leading edge.

When the aerofoil turns clockwise the moment would be positive. The moment coefficient is defined as:

$$C_m = \frac{M}{\frac{1}{2}\rho V^2 c^2}$$

The lift coefficient increases linearly with angle of attack, which is the angle between the chord line and the air flow. C_l increases at the rate of 2π/rad until the maximum value is reached, and the lift force starts to decrease. At this point the aerofoil is said to stall and the drag coefficient starts to increase rapidly. To generate the maximum lift/drag ratio, the optimum angle of attack should be set.

Therefore, unlike the above rated region where the pitch angle is used to decrease the angle of attack to discard the excess energy in the wind to generate rated power, pitch angle could be used in below rated region to increase the angle of attack to maximise the energy capture.

6.4. Control strategy designed to improve power capture in below rated wind speed

Having defined the control objective as improving the power capture in below rated region, and identified the best approach to using negative pitch angle to increase the angle of attack, the control strategy to achieve these criteria is configured as shown in Figure 6-3:

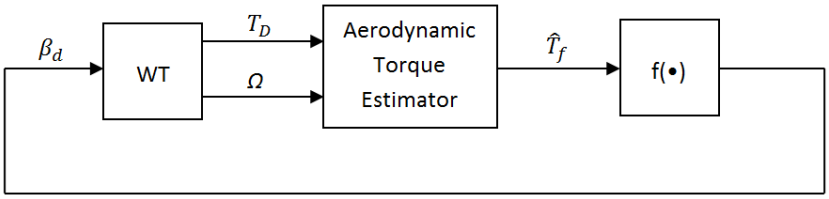

Figure 6-3: Control strategy designed to improve power capture

Where WT is the wind turbine model, T_D is the drive-train torque (generator torque), Ω is the rotor speed, $\hat{T}_f$ is the estimated aerodynamic torque and β_d is the pitch demand.

The control strategy requires drive-train torque (in this context generator torque) and the rotor speed measurements from the turbine and feeds them to an aerodynamic torque estimator. The estimated aerodynamic torque is then used to calculate the pitch angle demand and feed it back to turbine.

6.4.1. Aerodynamic estimator

As explained earlier it is convenient to use aerodynamic torque to indicate the operating state of the turbine, therefore, the estimated aerodynamic torque is used in the control strategy to set the best pitch angle.

The aerodynamic torque must be estimated as a function of drive train torque and rotor speed as it is not normally measurable. A possible estimator for the aerodynamic torque is of form of:

$$\hat{T}_f = NT_e + 10Q$$

$$\frac{dQ}{dt} + 10Q = (I_1 + N^2 I_2)\frac{dv}{dt} + (\gamma_1 + N^2\gamma_2)v$$

where $(I_1 + N^2 I_2)$ is the total drive train inertia and $(\gamma_1 + N^2\gamma_2)$ is the total viscous damping coefficients. Hence

$$h(s) = \frac{10((I_1+N^2 I_2)s+(\gamma_1+N^2\gamma_2))}{(s+10)}$$

N is gearbox ration (40.65), I_1 is rotor inertia ($1.9 * 10^5\ kgm^2$), I_2 is generator inertia ($3.8\ kgm^2$), $\gamma_1$is low speed shaft external damping coefficient (500 Nm/rad/s) and $\gamma_2$is high speed shaft external damping coefficient (0.3 Nm/rad/s)

The aerodynamic torque estimator was implemented in Simulink as depicted in Figure 6-4.

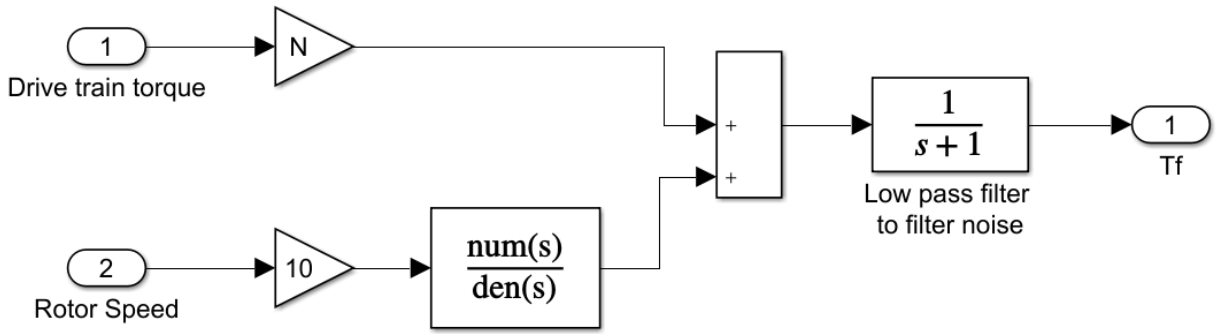

Figure 6-4: Aerodynamic torque estimator

The effectiveness of the estimator is established from Simulink simulations. As depicted in Figure 6-5, the estimated aerodynamic torque matches aerodynamic torque calculated from the wind model very closely.

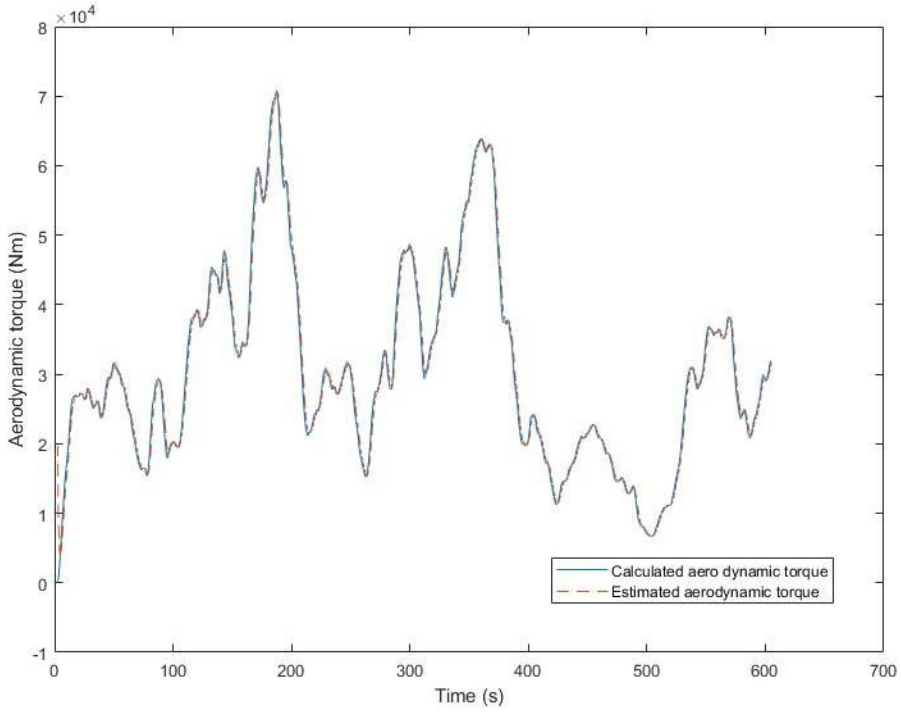

Figure 6-5: Aerodynamic torque

6.4.2. Determining the best pitch angle for different wind speed

To determine the best pitch angle for different wind speeds in below rated region, the $C_p$table that was discussed in chapter 5.1 is used. The objective is to make a look up table, which gives an output of pitch demand as a function of estimated aerodynamic torque. Therefore, from the 2MW Supergen exemplar wind turbine C_p table, the pitch angle which gives the highest value for $C_p$for each tip speed ratio can be determined. By running the simulation and setting constant wind speed (with 0 turbulence intensity) the tip speed ratio can be recorded for each wind speed and then according to the tip speed ratio the best pitch angle can be selected to give the highest C_p value. The estimated value of aerodynamic torque can be recorded by running the simulation using the best pitch angle. The procedure was repeated in steps of 0.2 for below rated wind speeds and the results are tabulated in Table 6-1:

Table 6-1: Pitch angle look up table

WS	Ω	λ	C_p	β	$\hat{T}_f$
6.0	3.871	10.65	0.459	-1.0	$1.342 * 10^4$
6.2	3.872	10.3	0.4623	-1.0	$1.491 * 10^4$
6.4	3.873	9.985	0.4644	-1.0	$1.645 * 10^4$
6.6	3.874	9.685	0.4662	-1.5	$1.813 * 10^4$
6.8	3.875	9.403	0.4677	-1.5	$1.988 * 10^4$
7.0	3.876	9.136	0.4687	-1.5	$2.173 * 10^4$
7.2	3.877	8.885	0.4697	-2.0	$2.368 * 10^4$
7.4	3.879	8.649	0.4704	-2.0	$2.572 * 10^4$
7.6	3.88	8.424	0.4712	-2.5	$2.793 * 10^4$
7.8	3.882	8.212	0.4721	-2.5	$3.022 * 10^4$
8.0	3.883	8.009	0.4728	-3.0	$3.265 * 10^4$
8.2	3.885	7.817	0.4735	-3.0	$3.508 * 10^4$
8.4	3.886	7.633	0.4695	-3.0	$3.746 * 10^4$
8.6	3.888	7.46	0.4686	-3.5	$4.014 * 10^4$
8.8	3.89	7.294	0.4679	-3.5	$4.291 * 10^4$
9.0	3.892	7.135	0.4664	-4.0	$4.577 * 10^4$
9.2	3.894	6.984	0.4649	-4.0	$4.868 * 10^4$
9.4	3.896	6.839	0.465	-4.5	$5.17 * 10^4$
9.6	3.898	6.7	0.4613	-5.0	$5.483 * 10^4$

9.8	3.9	6.566	0.4581	-4.5	$5.782 * 10^4$
10.0	3.901	6.437	0.4515	-4.0	$6.029 * 10^4$
10.2	3.903	6.314	0.4434	-5.0	$6.315 * 10^4$
10.4	3.905	6.195	0.4387	-5.0	$6.619 * 10^4$
10.6	3.908	6.082	0.435	-5.0	$6.945 * 10^4$
10.8	3.91	5.974	0.4303	-5.0	$7.263 * 10^4$
11.0	3.911	5.868	0.4233	-5.0	$7.548 * 10^4$
11.2	3.913	5.765	0.4169	-4.5	$7.831 * 10^4$
11.4	3.915	5.666	0.4117	-4.0	$8.157 * 10^4$
11.6	3.917	5.572	0.4012	-4.0	$8.37 * 10^4$
11.8	3.919	5.48	0.3933	-3.5	$8.632 * 10^4$
12.0	3.92	5.39	0.3849	-3.0	$8.887 * 10^4$

The data shown in Table 6-1 is used to create the pitch angle look up table for the control loop. However, the pitch demand cannot be used directly to feed to C_p table. The actual pitch angle which should be used is the output of the pitch actuator.

The pitch actuator can be modelled by a simplified linear first order transfer function as:

$$Actuator = \frac{25.9}{(s+25.9)}$$

6.4.3. Pitch rate

The rate of change of pitch angle should also be calculated because it should be considered that the control strategy does not introduce excessive pitch activity to the wind turbine operation. Excessive pitch activity may result in fatigue in the pitch motors and increase the risk of pitch system failure as well as wasting some of the extra power capture.

The pitch rate can be calculated as the derivative of pitch angle; therefore, it can be obtained by feeding the pitch angle into a derivative term in the Simulink model and monitoring the result. Running the simulation at 8m/s wind speed with 20% turbulence intensity provided the pitch rates which are plotted in Figure 6-6:

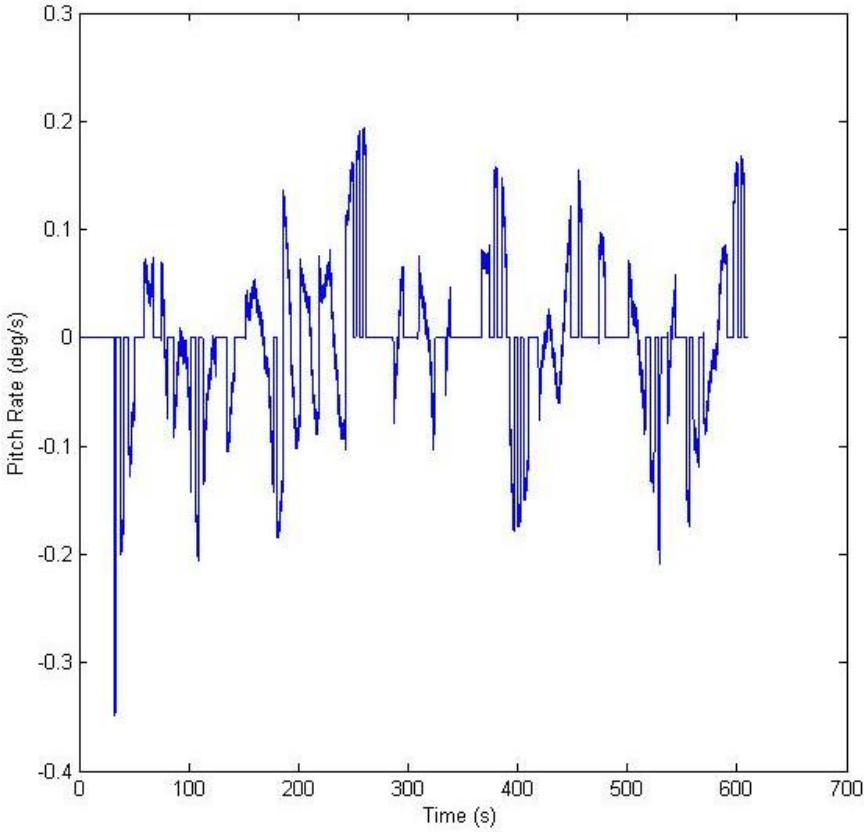

Figure 6-6: Pitch rate

From the simulation data shown in Figure 6-6, it can be observed that there are some rapid fluctuations which result in rapid changes in pitch motor. Constant changes in direction of actuator result in inducing excess mechanical loads on the component which leads to wear and tear and reduction of the lifetime of the pitch actuator and bearings. Based on these criteria, the pitch system may need to be upgraded. Any requirement to upgrade the pitch actuator and bearings will come at a cost, and this potential cost need to be compared with the benefit gained from the increased power capture using the control strategy introduced in this thesis.

7. Results

7.1. Estimation of improvement in power

To obtain a good estimation of whether the control strategy designed can in fact improve the power capture of constant speed wind turbines in below rated region, power capture is calculated over a 10 minutes simulation.

The power is calculated in different scenarios e.g. with different mean wind speeds in below rated, with 10%, 15% and 20% turbulence intensity. Each scenario should be simulated for both with and without the control system, and then determine the difference in power.

7.1.1. Theoretical power capture

Theoretically, the power capture by a wind turbine is calculated using the following equation:

$$P = \frac{1}{2}\rho\pi R^2 v^3 C_p(\lambda, \beta)$$

ρ is air density, R is radius of rotor (16.5 used here), v is the wind speed and C_p is the power coefficient in function of tip speed ratio (λ) and pitch angle (β).

The simulation is run with different constant wind speeds. To observe the effect of fixed and variable pitch angles on power capture, the simulation is run for each wind speed with having pitch angle fixed at 0, -2,-3 and also varying the pitch angle using the control system.

The implemented wind turbine model in the simulation provides the rotor speed which can be used to calculate the tip speed ratio using the following equation:

$$\lambda = \frac{\Omega R}{v}$$

Ω is the rotor speed, R is radius of rotor (16.5 used here) and v is the wind speed.

The value of C_p is obtained from the look up table explained in section 5.1, the full table is available in the Appendix B, according to the calculated tip speed ratio and for each of the fixed pitch and variable pitch angles. Feeding the calculated values to the power capture equation, the theoretical power capture by the wind turbine is calculated for each wind speed. The calculation is repeated for wind speeds incrementing in steps of 0.2m/s. The results are tabulated in Table 7-1:

Table 7-1: Theoretical power capture

Wind speed (m/s)	Power (W), β = -3°	Power (W), β = -2°	Power (W), β = -0°	Power (W),	β=varying(°)
6.00	48986.03	51146.99	50876.09	51935.35	-1.0
6.20	54955.08	57040.78	56419.45	57716.26	-1.0
6.40	61318.55	63239.90	62217.13	63770.44	-1.0
6.60	68071.63	69862.67	68219.06	70213.25	-1.5
6.80	75192.51	76823.29	74438.44	77038.90	-1.5
7.00	82775.16	84144.61	81034.49	84217.78	-1.5
7.20	90743.32	91833.84	87909.70	91833.82	-2.0
7.40	99099.31	99870.56	95088.12	99868.69	-2.0
7.60	107938.05	108262.72	102564.33	108355.04	-2.5
7.80	117166.84	116973.59	110281.41	117356.36	-2.5
8.00	126797.89	126024.87	118307.20	126797.89	-3.0
8.20	136758.28	135333.88	126656.25	136758.33	-3.0
8.40	145791.42	145015.23	135281.51	145791.42	-3.0
8.60	155948.65	153684.79	144231.17	156148.31	-3.5
8.80	166585.54	163573.30	153461.70	167062.05	-3.5
9.00	177402.64	173985.59	162122.97	178141.44	-4.0
9.20	188352.24	184726.57	171318.59	189665.88	-4.0
9.40	199407.98	195747.19	181275.71	201439.67	-4.5
9.60	210730.60	206961.53	191669.75	213795.31	-5.0
9.80	222299.18	218166.26	202367.62	225848.49	-4.5
10.00	234076.02	229449.42	213400.77	236582.54	-4.0
10.20	245719.32	240980.59	224717.23	246480.70	-5.0
10.40	256987.43	252750.66	236190.73	258503.84	-5.0
10.60	265862.58	263745.39	247982.09	271381.37	-5.0
10.80	277070.97	273957.12	259951.93	283973.64	-5.0
11.00	288821.02	283628.57	271775.81	295213.86	-5.0
11.20	301097.55	295110.77	282973.10	306843.94	-4.5
11.40	313734.50	306936.43	293440.12	319631.91	-4.0
11.60	325890.40	319269.38	303235.90	328072.95	-4.0
11.80	330000.00	330000.00	313982.91	330000.00	-3.5
12.00	330000.00	330000.00	325576.29	330000.00	-3.0

The wind turbine parameters used to run the simulation are for a three bladed 330kW with the following values:

$D_e = 915.8\ Nm/rad/s$

$I_1 = 1.9 * 10^5\ kgm^2$

$I_2 = 3.8\ kgm^2$

$K_1 = 1.26 * 10^7\ Nm/rad$

$K_2 = 3.02 * 10^5\ Nm/rad$

$\tau = 0.03\ s$

$N = 40.65$

$\gamma_1 = 500$

$\gamma_2 = 0.3$

Therefore, the power output in the simulation should be capped to 330 kW. Since the simulation does not include above rated power regulation, a saturation block is used to keep the power at rated when the wind speed exceeds the rated values (12m/s).

The average of the improvement of power with using the controller compared to use of different fixed pitch angles is obtained by calculating the mean value of the power captured for the whole range of wind speeds for each of the fixed pitch angles and comparing the difference against the power capture using the variable pitch. The results are tabulated in Table 7-2:

Table 7-2: Power capture improvement

Improvement compared to -3° pitch angle	1.4285%
Improvement compared to -2° pitch angle	1.8758%
Improvement compared to 0° pitch angle	7.3219%

The power curves produced from the calculated power capture from the simulations is depicted in Figure 7-1. Of course, it should be noted that the simulation is carried out only in below rated and the assumption is made that the turbine includes an above rated control system which would regulate the power capture in above rated region to keep the rated value.

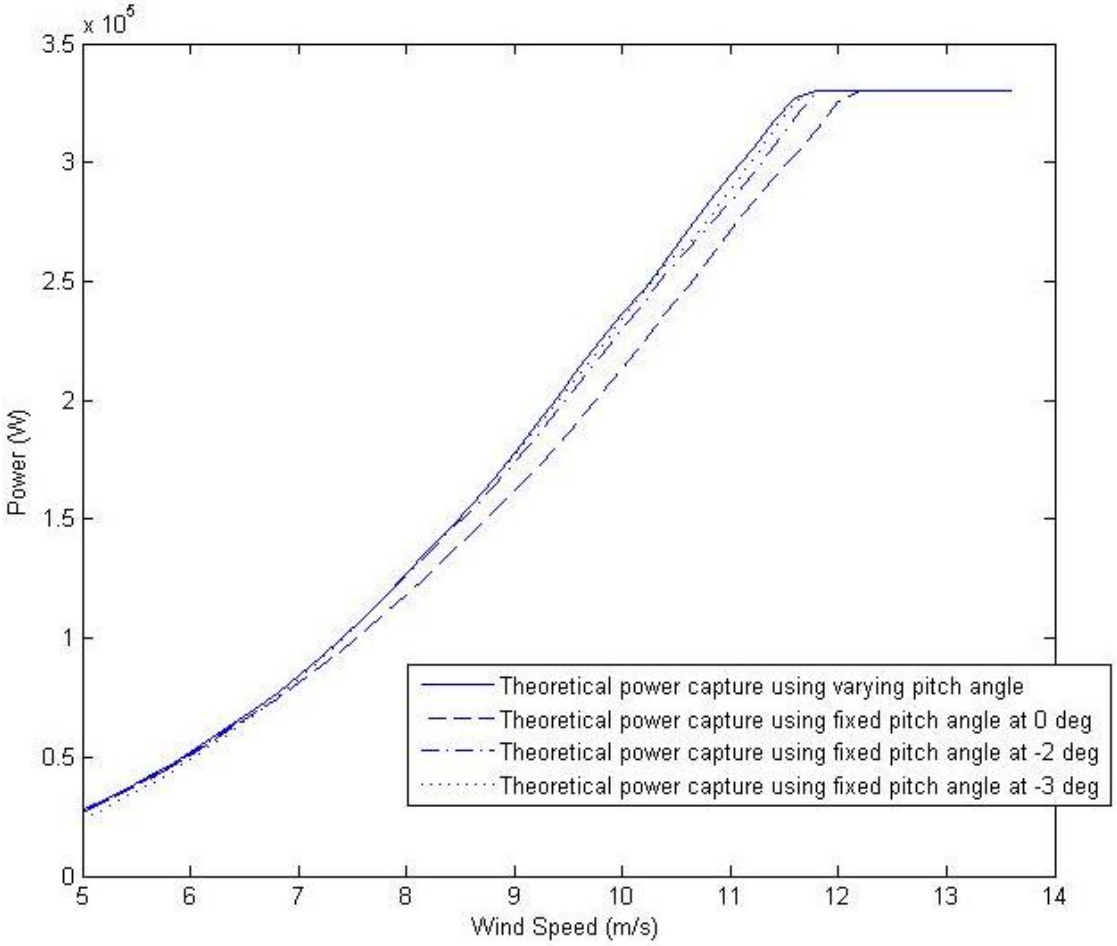

Figure 7-1: Theoretical power curves

It should also be noted that the fixed pitch angle in below rated wind speed used by the 2MW Supergen exemplar wind turbine is -3 deg.

7.1.2. Electrical power generated

The electrical power should now be calculated using wind with turbulence to achieve a more realistic insight into the control system performance and improvement compared to using a fixed pitch angle. The simulation is run with three different turbulence intensities set at 10%, 15% and 20%. Of course, the more realistic evaluation is to calculate the turbulence intensity specifically for every wind speed. This would need parameters relating to the class of the turbines but these are not available to use. However, for the purpose of comparison of power curves, the approach of keeping the turbulence intensity constant over the range of wind speeds and changing the standard deviation is sufficient. The relationship of turbulence intensity with standard deviation and wind speed is

$$I = \frac{\sigma_v}{\bar{V}}$$

where I is the turbulence intensity, σ_v is the standard deviation and $\bar{V}$ is the mean wind speed.

The power calculated with the constant wind speed would be the ideal value. To obtain a more realistic insight, it is better to use the electrical power output from the simulation, which is obtained by

$$P = generator\ torue * generator\ speed$$

As observed from the result, tabulated in Table 7-2, the pitch angle of -3 degrees provides the most power capture between the different fixed pitch angles tested. Therefore, it is sufficient to compare the results with the control system against the simulation using only -3 degrees as the fixed pitch angle.

The simulation is performed for different mean wind speeds in steps of 1m/s. The power output values for each wind speed are the bins of 10 runs of over 10 minutes. To generate different wind for every simulation a random number is used for the White Noise Seed in wind model. The average of the output power is used to plot the power curve. The results are tabulated in Table 7-3:

Table 7-3: Power output

Mean wind speed (m/s)	Power, fixed pitch, 10% turbulence (W)	Power, var pitch, 10% turbulence (W)	Power, fixed pitch, 15% turbulence (W)	Power, var pitch, 15% turbulence (W)	Power, fixed pitch, 20% turbulence (W)	Power, var pitch, 20% turbulence (W)
6	36819.31	39488.47	39369.18	41750.68	32626.38	35157.22
7	67741.80	69090.68	71270.26	72627.42	76107.64	77497.25
8	112020.09	112348.96	108941.90	109511.38	119562.05	120228.21
9	166109.11	166832.69	164923.43	165674.91	159560.95	159760.31
10	218978.35	220722.88	228871.10	230468.37	225156.66	226666.90
11	277287.40	279394.86	282437.77	283460.65	272082.70	273310.21
12	318829.01	319138.54	313677.33	314226.13	304277.87	304455.36

The percentage of the improvement of power capture are calculated in the same manner as the theoretical power improvement with using the mean value of the power captured for the whole range of wind speeds for the fixed pitch angle and comparing the difference against the power capture using the variable pitch controller. This is repeated for the three different values of turbulence intensities used. The results are tabulated in Table 7-4:

Table 7-4: Power capture improvement

Improvement in power capture in 10% turbulence	1.6605 %
Improvement in power capture in 15% turbulence	1.4524 %
Improvement in power capture in 20% turbulence	1.635 %

It should be mentioned that the electrical losses are neglected here, in other words the efficiency, K_{eff}, is assumed to be 1.

The binned values of output power are used to plot the power curve to have fairly accurate observation. The power curves for these results are depicted in Figure 7-2:

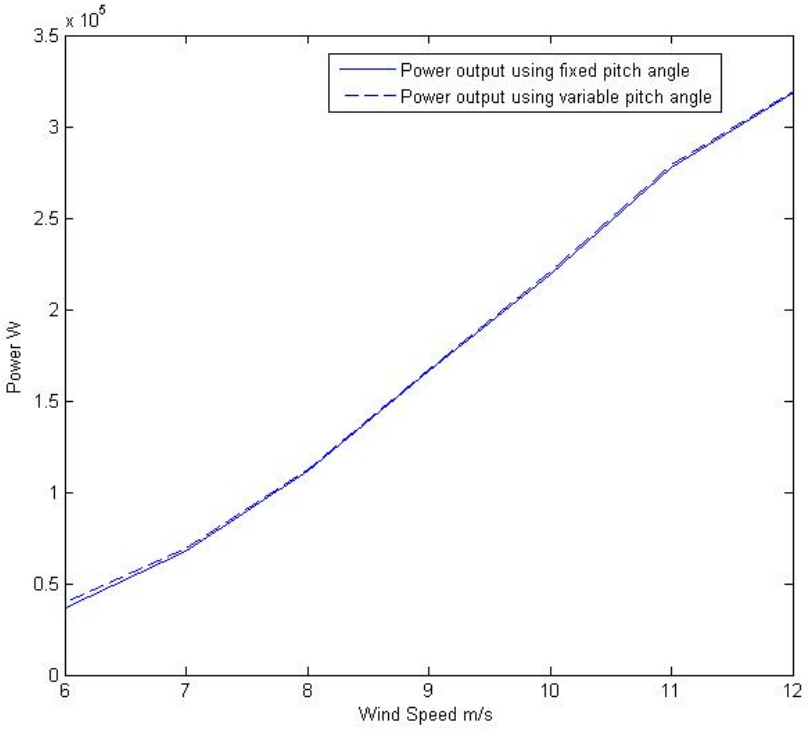

a) Power curve produced from wind speed with 10% turbulence intensity

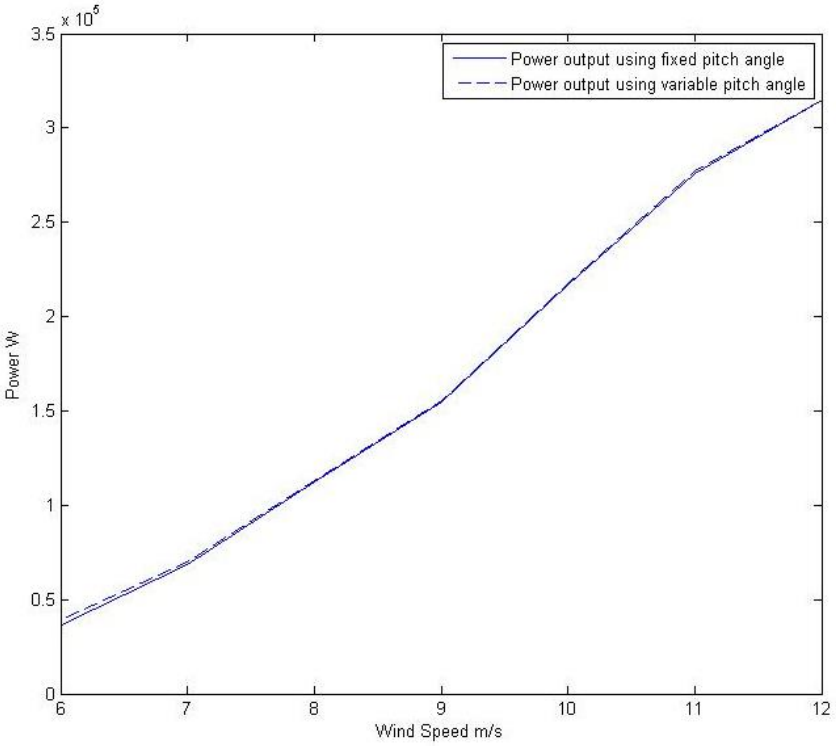

b) Power curve produced from wind speed with 15% turbulence intensity

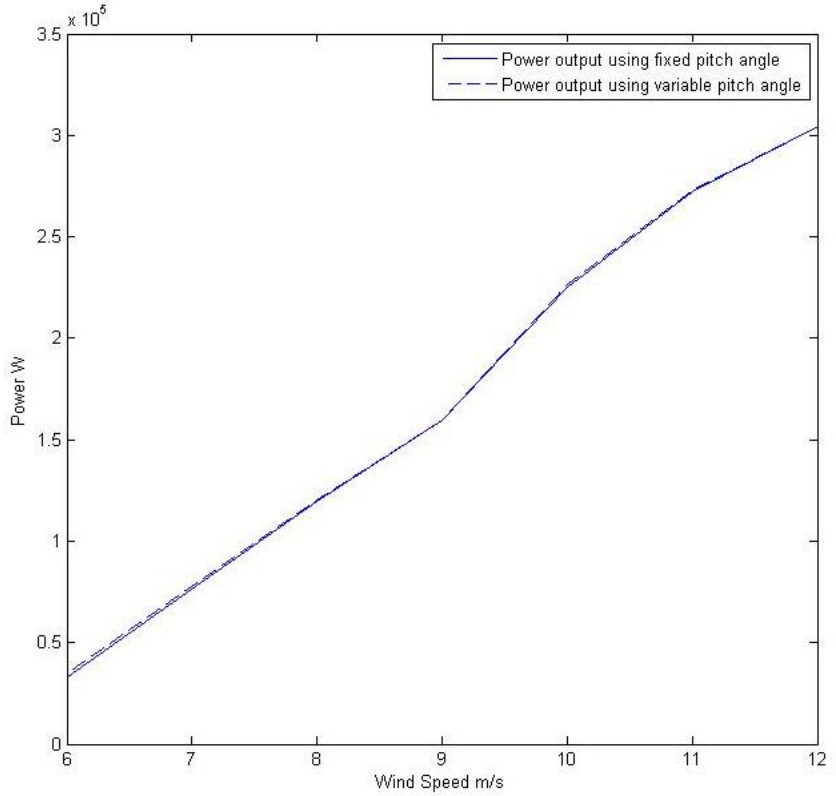

c) Power curve produced from wind speed with 20% turbulence intensity

Figure 7-2 : Power curves

As shown in Figure 7-3 it can be observed that the most improvement is at lower wind speeds.

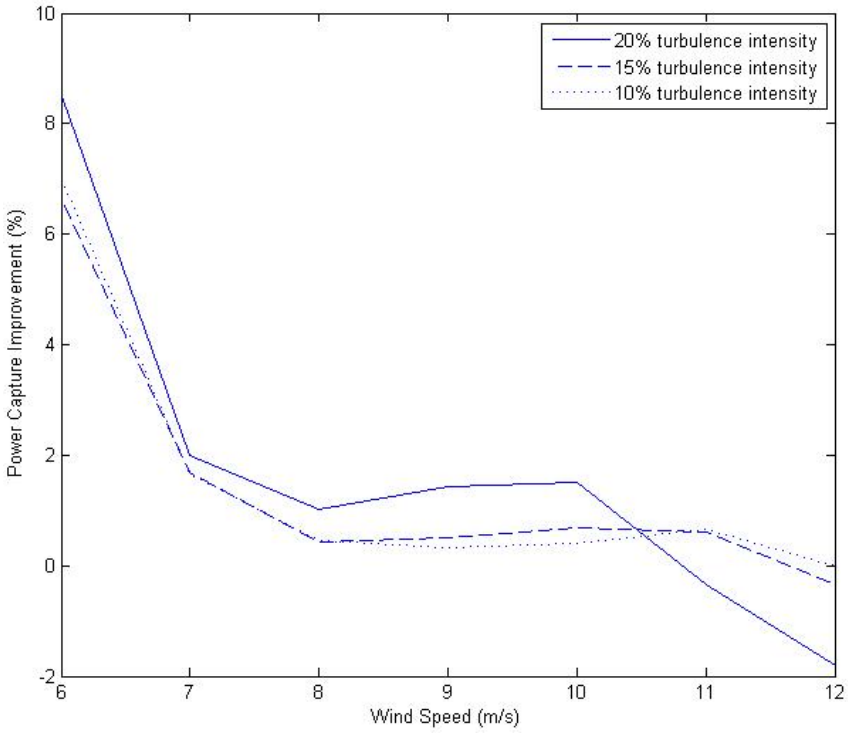

Figure 7-3: Power improvement vs wind speeds with different turbulence intensity

7.2. Annual energy yield calculation

It is important to account for the behaviour of the wind in order to achieve an accurate prediction of wind turbine performance. The most important characteristic of the wind is its variabilities. The continuous and stochastic variations of the wind can be analysed in different time scales such as yearly, seasonal, daily and even, when considering the turbulent, the variations can be second to second. The commonly used Van der Hoven spectrum, Figure 7-4, demonstrates the variation in wind over the time scales mentioned.

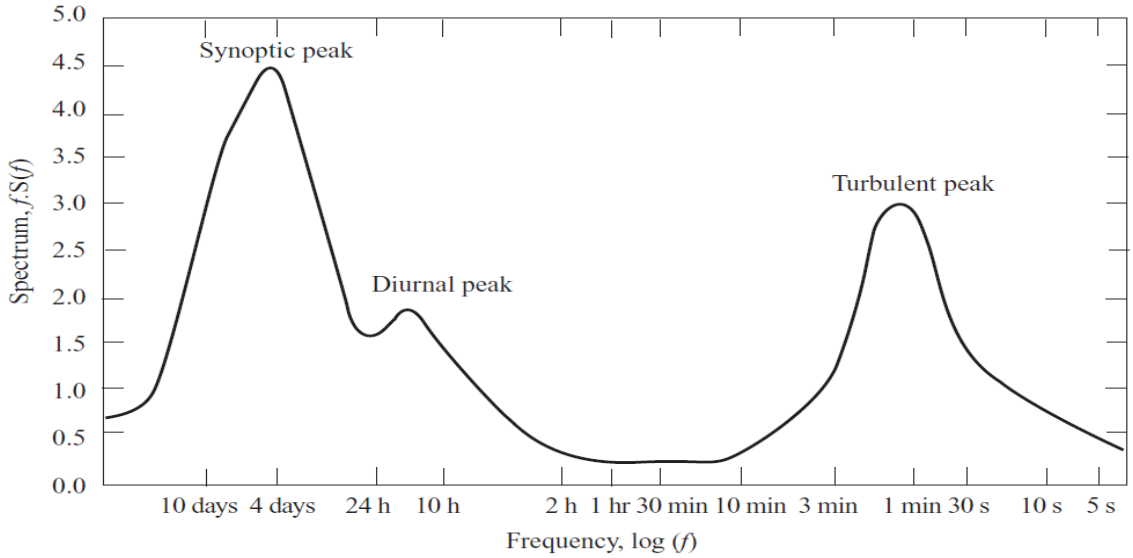

Figure 7-4: Van der Hoven spectrum

The spectrum depicted in Figure 7-4, demonstrates that the variation of wind in time scales of 10mins to 2hr is quite low.

7.2.1. Annual and seasonal variation

An appropriate approach to characterising the annual variation of wind speed is to use a probability distribution. The Weibull distribution is suitable for representing hourly variation of mean wind speed over a year. The Weibull distribution is represented by

$$F(U) = \exp\left(-(\frac{U}{c})^k\right)$$

where $F(U)$ is the fraction of time for which the hourly mean wind speed exceeds U, c is the scale parameter and k is the shape parameter.

The annual mean wind speed $\overline{U}$ and c are related by

$$\overline{U} = c\Gamma\left(1 + \frac{1}{k}\right)$$

Γ is the complete gamma function. The probability density function is

$$f(U) = -\frac{dF(U)}{dU} = k\frac{U^{k-1}}{c^k}\exp\left(-(\frac{U}{c})^k\right)$$

with mean wind speed is derived by:

$$\overline{U} = \int_0^\infty Uf(U)dU$$

The Rayleigh distribution is a special case of Weibull distribution, for which $k = 2$ and $\Gamma\left(1 + \frac{1}{k}\right) = \sqrt{\frac{\pi}{2}} = 0.8862$. These values are fairly common for many locations.

The locations with small variation of hourly mean wind speed relative to annual mean wind speed have higher value of k, such as 2.5 or 3, and the sites with greater variation have smaller value of k, such as 1.5 or 1.2. Some examples are given in Figure 7-5:

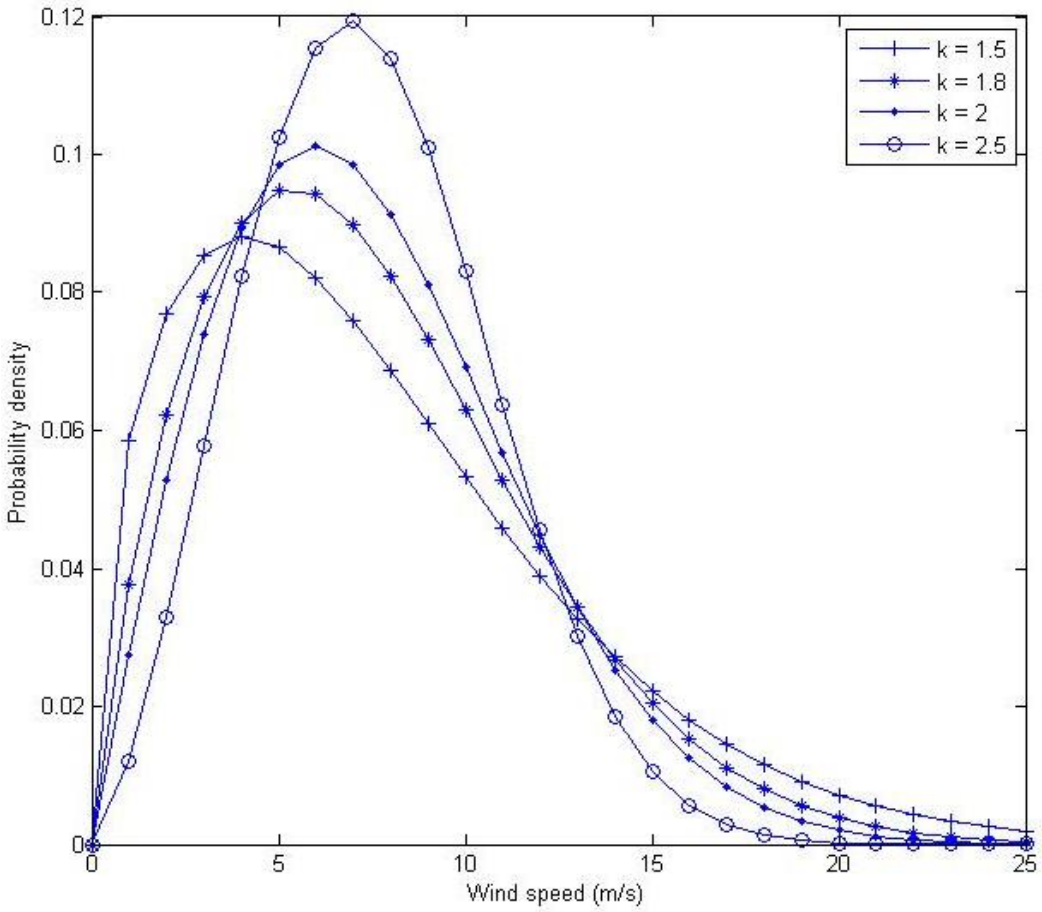

Figure 7-5: Weibull distributions density

Despite the fact that Weibull distribution represents the wind regime appropriately at many locations, it should still be noted that some sites can have completely different climates in summer and winter. For these sites double-peaked 'bi-Weibull' distributions can be used to properly represent the wind regime. Bi-Weibull distribution has different scale factors and shape factors in the two seasons as follow:

$$F(U) = F_1 \exp\left(-(\frac{U}{c_1})^{k_1}\right) + (1 - F_1) \exp\left(-(\frac{U}{c_2})^{k_2}\right)$$

7.2.2. Estimation of energy capture

The amount of energy capture by a wind turbine depends on the wind speed distribution at the location and the power versus the wind speed characterisation of the wind turbine.

Using the equations described in previous sections, the probability $F(U)$ that the wind speed lies between U_i and U_{i+1} is calculated as follow:

$$F(U) = \exp\left(-(\frac{U_i}{c})^k\right) - \exp\left(-(\frac{U_{i+1}}{c})^k\right)$$

with

$$c = \frac{7.5}{\sqrt{\frac{\pi}{2}}} = 8.4628 \quad \text{and} \quad \Gamma\left(1+\frac{1}{k}\right), \text{for } k = 2 \text{ is } \sqrt{\frac{\pi}{2}}$$

(Note: the value of U and k should be chosen based on the design of a turbine for a specific class. However, as there is no information available about the class of the design, the values of annual mean wind speed, $\bar{U}$, and the shape factor, k, are chosen to be 7.5m/s and 2, respectively. The chosen values correspond to turbine class of either A3 or B3).

The annual probability distribution function is shown in Figure 7-6. The values are calculated for the following range of wind speed:

$U_i = [0.5:1:24.5]$

$U_{i+1} = [1.5:1:25.5]$

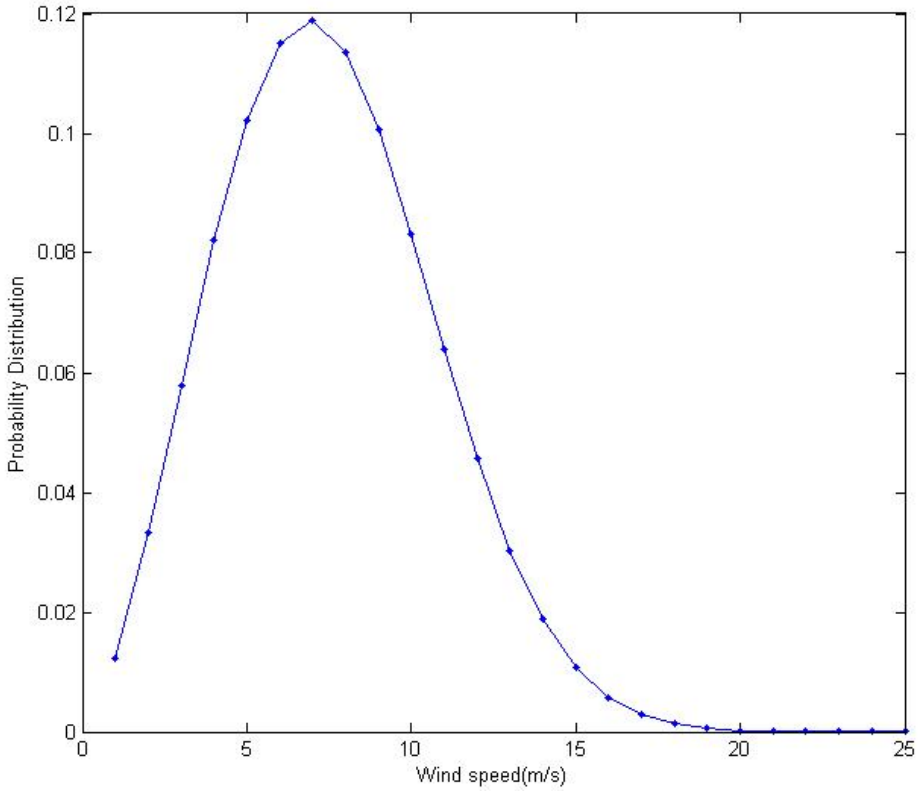

Figure 7-6: Weibull distributions

Using the power curve calculated from the power output in the previous section, the probability for the power to be generated in each wind speed is calculated as follow:

$$P = P(V_m) \int_{V_m-0.5}^{V_m+0.5} F(U)$$

The numerical integration above is solved using the Trapezoidal rule:

$$\mathrm{P} = \Sigma(\mathrm{P_{i+1}F(U_{i+1})} + \mathrm{P_i F(U_i)}) \frac{(\mathrm{U_{i+1}} - \mathrm{U_i})}{2}$$

To make an estimation of the annual energy yield, the daily energy capture is calculated. The Weibull distribution provides the probability of hourly wind speed about the annual mean wind speed. Therefore, by multiplying the region, for example 5.5 m/s to 6.6m/s, of Weibull distribution with the power production at that region, 6 m/s in this example, which is taken from the power curve, the hourly power production can be calculated. Then the hourly power should be multiplied by 24 to calculate the daily rate and then by the number of days in a year. However, turbines may not be running all the time due to maintenance and down time. The results are tabulated in Table 7-5:

Table 7-5: Annual energy yeild

Mean wind speed (m/s)	Power, fixed pitch, 10% turbulence (W/h)	Power, var pitch, 10% turbulence (W/h)	Power, fixed pitch, 15% turbulence (W/h)	Power, var pitch, 15% turbulence (W/h)	Power, fixed pitch, 20% turbulence (W/h)	Power, var pitch, 20% turbulence (W/h)
6	37127484.7	39818977.9	39698692.1	42100122.3	32899452.7	35451482.2
7	70552525.7	71957373.2	74227385.6	75640858.5	79265474.3	80712744.0
8	111439846.7	111767011.5	108377595.7	108944134.7	118942741.8	119605451.7
9	146562034.1	147200467.4	145515875.4	146178925.6	140784435.9	140960335.4
10	159418051.0	160688083.0	166620053.3	167782884.3	163915910.9	165015382.7
11	155054776.8	156233230.5	157934778.7	158506760.6	152144385.8	152830789.2
12	127463919.8	127587668.7	125404343.8	125623746.5	121646552.7	121717512.5
13	87740337.4	87740337.4	87740337.4	87740337.4	87740337.4	87740337.4
14	54227210.1	54227210.1	54227210.1	54227210.1	54227210.1	54227210.1
15	31108592.5	31108592.5	31108592.5	31108592.5	31108592.5	31108592.5
16	16542674.6	16542674.6	16542674.6	16542674.6	16542674.6	16542674.6
17	8142651.0	8142651.0	8142651.0	8142651.0	8142651.0	8142651.0
18	3704274.7	3704274.7	3704274.7	3704274.7	3704274.7	3704274.7
19	1555037.2	1555037.2	1555037.2	1555037.2	1555037.2	1555037.2
20	601435.9	601435.9	601435.9	601435.9	601435.9	601435.9
21	213969.9	213969.9	213969.9	213969.9	213969.9	213969.9
22	69908.7	69908.7	69908.7	69908.7	69908.7	69908.7
23	20942.4	20942.4	20942.4	20942.4	20942.4	20942.4
24	5743.0	5743.0	5743.0	5743.0	5743.0	5743.0
25	1439.4	1439.4	1439.4	1439.4	1439.4	1439.4

Improvement of energy yield per year is calculated and the results are tabulated in Table 7-6:

Table 7-6 : Annual enegy yield improvement

Improvement in annual energy yield per year with 10% turbulence	0.749 %
Improvement in annual energy yield per year with 15% turbulence	0.6803 %
Improvement in annual energy yield per year with 20% turbulence	0.6562 %

8. Conclusion

Using the Weibull probability distribution, it is clear that wind turbines spend the biggest percentage of their life time in below rated region. Therefore, improvement of power capture in this region could make the wind turbines more efficient.

The Simulink based simulations proved there is extra power capture when employing the control strategy using negative pitch angles in below rated region.

The concerns about having to utilise the wind turbine with excessive number of instruments, can be ruled out as all the required measurements for the control strategy are just rotor speed and generator torque, which are the inputs to the aerodynamic torque estimator. These two measurements are already employed in most of the running turbines and no further sensors or measuring equipment are necessary for this purpose which makes this approach cost effective.

The pitch rate for the control strategy which is proposed in this thesis is also assessed. The simulations carried out proved the fact that the pitch rate is very small and the power consumption due to the extra pitch activity in below rated is very small and will not waste the extra power capture.

Although the improvement in power capture would seem small, when considered over the 25 years life time of a wind turbine, significant amount of extra power can be captured. Also the wind turbine parameters used in this thesis correspond to a 330kW wind turbine, which is a small machine and considering the modern wind turbines, which can produce 5MW, the small percentage of improvement would be worthwhile.

References and bibliography

[1] Wilkie, J., Leithead, W.E., Anderson, C. *Modelling of the wind turbines by simple models,* Wind engineering Vol 14, 1990, pp 247-275

[2] Madsen, P.H., Frandsen, S. *Pitch angle control for power limitation.* Proc. Of European Wind Energy Conference, Hamburg, 2984, pp. 612-919.

[3] Robb, D.M., Leithead, W.E. *Derivation and validation of simple correlated wind speed.* Internal Report. Department of Electrical and Electronic Engineering, University of Strathclyde, Glasgow, Scotland.

[4] Davenport, A.G., *The spectrum of horizontal gustiness near the ground in high winds.* Quart. J. Roy. Met. Scot., 1961, 87, pp. 194-221.

[5] Burton, T., Sharpe, D., Jenkins, N., Bossanyi, E. *Wind energy handbook.* 2001, pp 478-479.

[6] British Wind Energy Association: *Annual Review 2009.*

[7] Leithead, W.E., Rogers, M.C.M. Leithead, W.E. *Drive train Characteristic of constant speed HAWT's, Part I – Representation by simple dynamic models.* Wind Engineering, Vol. 20, 1996, pp. 149-174.

[8] Leithead, W.E., Rogers, M.C.M. Leithead, W.E. *Drive train Characteristic of constant speed HAWT's, Part II – Simple characterisation of dynamics.* Wind Engineering, Vol. 20, 1996, pp. 175-201.

[9] Leithead, W.E., Connor, B. *Control of variable speed wind turbines: design task.* International Journal of Control, VOL. 73, 2000, pp. 1189-1212.

[10] Leithead, W.E., Connor, B. *Control of variable speed wind turbines: dynamic models.* International Journal of Control, VOL. 73, 2000, pp. 1173-1188.

[11] Greco, L., Testa, C., Salvatore, F. *Design oriented aerodynamic modelling of wind turbine performance.* Journal of Physics: Conference Series, 75, no. 1, 2007. ISSN: 1742-6588, doi: 10.1088/1742-6596/75/1/012011.

[12] Bindner, H. *Active control: wind turbine model.* Riso-R-920(EN), 1999, Riso National Laboratory, Roskilde, Denmark.

[13] Leithead, W.E., de la Salle, S., Reardon, D. *Wind turbine control objectives and design.* 1990, Proc. European Community Wind Energy Conference and Exhibition, Madrid, Spain.

[14] Leithead, W.E., Leith, D.J., *Implementation of wind turbine controllers.* International Journal of Control, VOL 66, 1997, pp. 349-380.

[15] Leithead, W.E., de la Salle, S., Reardon, D., Grimble, M., J., *Wind turbine modelling and control.* 1991, Presented at the LFE Control 91 Conference, Heriot Watt University.

[16] Martin O.L. Hansen, *Aerodynamics of wind turbine.* Second Edition, 2008.

[17] Leithead, W.E., de la Salle, S., Reardon, D., Grimble, M., J., *Wind turbine control systems modelling and design – Phase I + II.* Report prepared for Dep. of Energy, University of Strathclyde, 1991.

[18] Leith, D.J., Leithead, W.E., *Implementation of wind turbine controller.* International Journal of Control, Vol. 66, 1997, pp. 349-380.

[19] Shahan, Z, *History Of Wind Turbines*, 2014, Retrieved from https://www.renewableenergyworld.com/ugc/articles/2014/11/history-of-wind-turbines.html

[20] Renewables 2010: Global Status Report (REN21, GSR), *Renewable Energy Policy Network for the 21st Century*, 2010.

[21] UK Renewable Energy Industry: *Introduction and overview, STEM Choices 7. Industry Focus*, 2009, pp. 7.17-7.29.

[22] Leithead, W.E., de la Salle, S., Reardon, D., 1991 a, *Role and objectives of control for wind turbines, IEE proceedings Part C,* 138, pp. 135-148.

[23] Goodfellow, D., Smith, G., A., And Gardner, G., 1986, *Control Strategies for variable speed wind energy recovery. Proceedings of the 8th British Wind Energy Association Conference Cambridge UK,* pp. 219-228.

[24] Leithead, W.E., 1989, *Variable speed operation-does it have any advantages? Wind Engineering,* 13, pp. 302-314.

[25] Leithead, W.E., 1990, *Dependence of performance of variable speed wind turbines on turbulence, dynamics and control. IEE Proceedings Part C,* 137, pp. 403-413.

Appendix A

Figure 3-3 shows C_{p-max} curve for two different rotors, designed for the purpose of variable speed operation. Figure 3-3 (a) demonstrates the C_{p-max} curve for the rotor that has a broad $C_p - \lambda$ curve, which is a more suitable design for a pitch regulated machine.

Figure 3-3 (b) shows a C_{p-max} curve for the rotor that has a more peaked $C_p - \lambda$ curve, which is a more suitable design for a stall regulation machine.

The $C_p - \lambda$ curves for the two rotors are shown in Figure A-0-1 along with a typical $C_p - \lambda$ curve for a constant speed machine for comparison purposes.

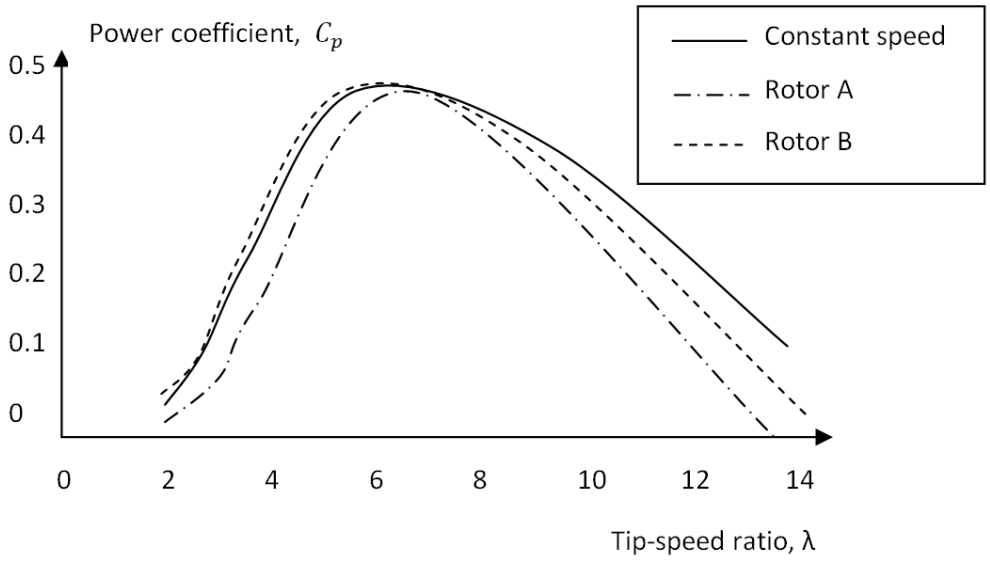

Figure A-0-1: $C_p - \lambda$ curve with flat (Rotor A) and peaked (Rotor B) characteristics

Appendix B

Supplementary data file

The C_p and C_t look up tables for the 2MW Supergen exemplar wind turbine are included as a supplementary data file on the CD-ROM enclosed to this thesis, as the tables are too large to be demonstrated in A4 size sheet in a readable format.

Filename:

2MW C_p C_t tables.xls